

LOCKHEED MARTIN ENERGY RESEARCH LIBRARIES



3 4456 0515942 2

CENTRAL RESEARCH LIBRARY  
DOCUMENT COLLECTION

3

ORNL-4090  
UC-80 - Reactor Technology

MEASUREMENTS AND SINGLE-VELOCITY  
CALCULATIONS OF DIFFERENTIAL ANGULAR  
THERMAL-NEUTRON ALBEDOS FOR CONCRETE

R. E. Maerker  
F. J. Muckenthaler

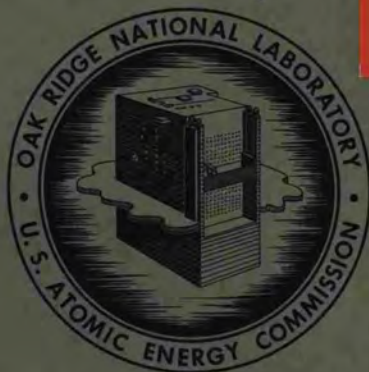
OAK RIDGE NATIONAL LABORATORY  
CENTRAL RESEARCH LIBRARY  
DOCUMENT COLLECTION

**LIBRARY LOAN COPY**

DO NOT TRANSFER TO ANOTHER PERSON

If you wish someone else to see this  
document, send in name with document  
and the library will arrange a loan.

UCN-7969  
(3 3-67)



**OAK RIDGE NATIONAL LABORATORY**  
operated by  
**UNION CARBIDE CORPORATION**  
for the  
**U.S. ATOMIC ENERGY COMMISSION**

Printed in the United States of America. Available from Clearinghouse for Federal  
Scientific and Technical Information, National Bureau of Standards,  
U.S. Department of Commerce, Springfield, Virginia 22151  
Price: Printed Copy \$3.00; Microfiche \$0.65

— LEGAL NOTICE —

This report was prepared as an account of Government sponsored work. Neither the United States, nor the Commission, nor any person acting on behalf of the Commission:

- A. Makes any warranty or representation, expressed or implied, with respect to the accuracy, completeness, or usefulness of the information contained in this report, or that the use of any information, apparatus, method, or process disclosed in this report may not infringe privately owned rights; or
- B. Assumes any liabilities with respect to the use of, or for damages resulting from the use of any information, apparatus, method, or process disclosed in this report.

As used in the above, "person acting on behalf of the Commission" includes any employee or contractor of the Commission, or employee of such contractor, to the extent that such employee or contractor of the Commission, or employee of such contractor prepares, disseminates, or provides access to, any information pursuant to his employment or contract with the Commission, or his employment with such contractor.

Contract No. W-7405-eng-26

Neutron Physics Division

MEASUREMENTS AND SINGLE-VELOCITY CALCULATIONS OF DIFFERENTIAL  
ANGULAR THERMAL-NEUTRON ALBEDOS FOR CONCRETE \*

R. E. Maerker and F. J. Muckenthaler

NOTE:

This Work Supported by  
DEFENSE ATOMIC SUPPORT AGENCY  
Under Orders EO-802-65 and EO-800-64

\*An abbreviated version of this report was published in Nucl. Sci. Eng.  
26, 339 (1966) and as ORNL TM-1421.

JULY 1967

OAK RIDGE NATIONAL LABORATORY  
Oak Ridge, Tennessee  
operated by  
UNION CARBIDE CORPORATION  
for the  
U. S. ATOMIC ENERGY COMMISSION

LOCKHEED MARTIN ENERGY RESEARCH LIBRARIES



3 4456 0515942 2

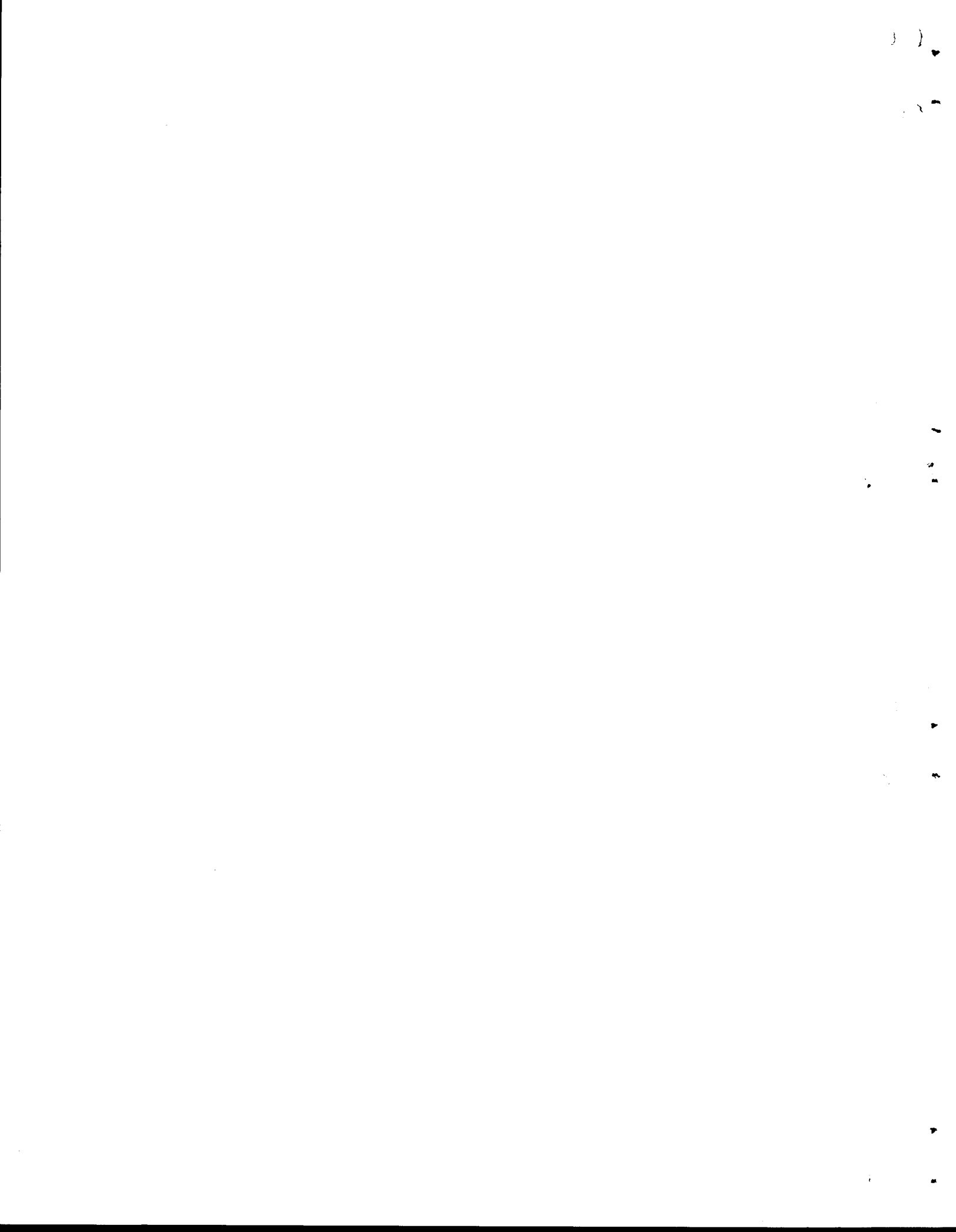


## TABLE OF CONTENTS

	<u>Page No.</u>
Abstract -----	iv
I. Introduction -----	1
II. Feasibility of Monte Carlo Technique for Calculating Thermal-Neutron Albedos -----	2
III. Comparison of Experiment with Calculations Including Presence of Iron Reinforcing -----	22
IV. Simple Albedo Expressions -----	41
Appendix -----	45

## ABSTRACT

Measurements and single-velocity Monte Carlo calculations have been performed to determine the differential angular thermal-neutron albedos for a reinforced concrete from monodirectional beams of incident thermal neutrons. Preliminary calculations using a statistical estimation technique indicate up to 50 scatterings should be followed for each neutron in order to produce good estimates of the differential albedos, and up to 100 scatterings to produce good estimates of the capture gamma-ray differential dose albedos. Deviation between experiment and calculation can be reduced to an average of 5.1% for 72 points of comparison if an anisotropic scattering law for water deduced from earlier Argonne National Laboratory measurements is assumed.

## I. INTRODUCTION

The work reported in this paper is part of a continuing program to determine neutron albedos for concrete. These albedos are differential both in angle and, with the exception of thermal neutrons, in energy and are to be used in Monte Carlo calculations of the transmission of neutrons through concrete-lined ducts in complex shielding structures. In the duct calculations the walls of the duct will be treated as surfaces having reflecting properties determined by the calculated differential albedos. The albedo results for fast neutrons were published previously,<sup>1</sup> and the results given here are for thermal neutrons.

This report has a threefold purpose. First, results are presented to demonstrate the feasibility of using the Monte Carlo method employed in conjunction with a statistical estimation technique in calculating thermal-neutron differential angular albedos and capture distributions for a semi-infinite weakly capturing medium such as concrete for the case of an incident broad beam of monodirectional and monoenergetic (0.025-eV) neutrons. A criterion is established for the approximate number of scatterings through which a particle must be followed before its subsequent contribution to the answer can be safely neglected. Second, the calculated results are compared with results from very precise experiments at the Tower Shielding Facility (TSF) at Oak Ridge National Laboratory to show to what extent a single-velocity approximation, using energy-independent scattering and absorption parameters, is adequate for treating the diffusion of subcadmium neutrons in a weakly absorbing medium. The anisotropy

---

1. R. E. Maerker and F. J. Muckenthaler, Differential Fast-Neutron Albedos for Concrete, Vols. I-VI, ORNL-3822 (1965).

of the scattering process can be reasonably deduced, as well. Third, simple formulas are presented which describe the differential angular albedo of plane parallel beams of subcadmium neutrons which agree quite well with measurement and calculation. Calculations of the differential capture gamma-ray angular current, in dose units, leaving the incident surface are also presented, as well as a fit with a simple formula for these data.

## II. FEASIBILITY OF MONTE CARLO TECHNIQUE FOR CALCULATING THERMAL-NEUTRON ALBEDOS

Preliminary calculations were performed to investigate the accuracy of the Monte Carlo technique using a single-velocity treatment for calculating differential angular albedos for thermal neutrons reflected from concrete, as well as capture gamma-ray source distributions within concrete. Although the technique was to be utilized later to analyze TSF experiments employing a concrete slab that had steel reinforcing bars in some regions, it was found by homogenizing each of the two 1-in. regions of the experimental slab that the 0.025-eV value of  $\Sigma_s/\Sigma_T$  is relatively insensitive to the presence of the steel (see Table 1); therefore, a spatially independent value of  $\Sigma_s/\Sigma_T$  was used in the preliminary calculations.\*

The geometry for these calculations, and for all subsequent calculations, is shown in Fig. 1. In general, the incident angles  $\theta_0$  that were used were 0, 45, 60, 75, and 90 deg.\*\* The reflected thermal-neutron

---

\*M. B. Wells analyzed two different concretes and obtained  $\Sigma_s/\Sigma_T$  values of 0.985 and 0.986 (see ref. 7). The value of  $\Sigma_s/\Sigma_T$  for the reinforced concrete in this paper, spatially averaged over the entire slab, is 0.985. Apparently this ratio is insensitive to the composition of the concrete for many types of concrete.

\*\*The 90-deg case was actually calculated for  $\theta_0 = \cos^{-1} 0.0001 \approx 89^\circ 59.7'$ .

Table 1. Composition of Concrete  
(6.0 wt% H<sub>2</sub>O;  $\rho = 2.30 \text{ g/cm}^3$ )

Element	Ordinary Concrete <sup>a</sup> (atoms/cm <sup>3</sup> )	Reinforced Concrete <sup>b</sup> (atoms/cm <sup>3</sup> )
Hydrogen	$8.50 \times 10^{21}$	$8.22 \times 10^{21}$
Carbon	$2.02 \times 10^{22}$	$1.95 \times 10^{22}$
Oxygen	$3.55 \times 10^{22}$	$3.43 \times 10^{22}$
Calcium	$1.11 \times 10^{22}$	$1.08 \times 10^{22}$
Silicon	$1.70 \times 10^{21}$	$1.64 \times 10^{21}$
Magnesium	$1.86 \times 10^{21}$	$1.80 \times 10^{21}$
Iron	$1.93 \times 10^{20}$	$2.96 \times 10^{21}$
Aluminum	$5.56 \times 10^{20}$	$5.38 \times 10^{20}$
Potassium	$4.03 \times 10^{19}$	$3.95 \times 10^{19}$
Sodium	$1.63 \times 10^{19}$	$1.58 \times 10^{19}$

a.  $\Sigma_S/\Sigma_T (0.025 \text{ eV}) = 0.987$ .

b.  $\Sigma_S/\Sigma_T (0.025 \text{ eV}) = 0.978$ ; composition of homogenized region closest to front face.

ORNL-DWG 65-11004R

REFLECTED NEUTRONS/STERADIAN/INCIDENT NEUTRON  
CALCULATED AT  $\cos \theta = -\frac{i+0.5}{9}$ ,  $i = 0 \rightarrow 8$   
 $\phi = 15 \text{ deg} + (30 \text{ deg}) i$ ,  $i = 0 \rightarrow 5$   
FOR  $\theta_0 = 0, 45, 60, 75, \text{ AND } 90 \text{ deg}$

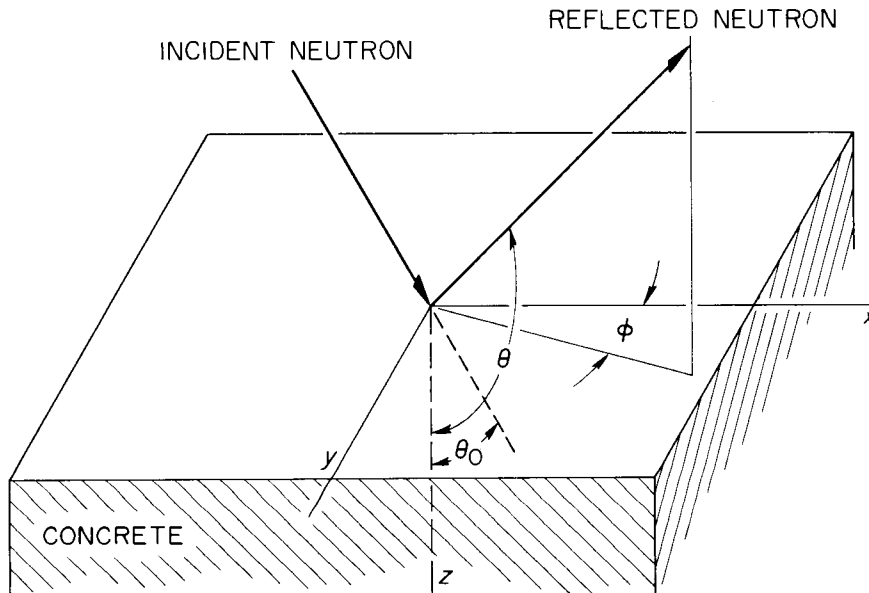


Fig. 1. Geometry Used for Monte Carlo Calculations of Thermal-Neutron Albedos for Concrete.

angular current was calculated for each of nine polar angles  $\theta$  and six azimuthal angles  $\phi$  describing the reflected direction. A technique of statistical estimation was used at each collision in a manner analogous to that described earlier for fast neutrons.<sup>1</sup>

Table 2 shows a comparison of the differential angular albedos (i.e., reflected neutron per steradian per incident source neutron) for the case of  $\Sigma_s/\Sigma_T = 0.975$ , a semi-infinite medium, isotropic scattering in the laboratory system, and a normally incident beam of neutrons with the exact results of Chandrasekhar<sup>2</sup> calculated from the expression

$$\frac{d\alpha}{d\Omega} = \frac{0.975}{4\pi} \frac{|\mu|}{|\mu| + 1} H(0.975, 1) H(0.975, |\mu|) ,$$

where  $|\mu| = |\cos\theta|$ , and  $H(\tilde{\omega}_0, |\mu|)$  satisfies the nonlinear integral equation:

$$H(\tilde{\omega}_0, |\mu|) = 1 + 0.5 \tilde{\omega}_0 |\mu| H(\tilde{\omega}_0, |\mu|) \int_0^1 \frac{H(\tilde{\omega}_0, |\mu'|)}{|\mu| + |\mu'|} d|\mu'| .$$

A correlated sampling technique, in which the cumulative score over collisions of each of the differential albedos was tabulated for various orders of scattering for each history, was used to calculate the albedos as cumulative functions of the maximum number of allowed scatterings of each neutron.

Differential angular albedos obtained from a similar calculation but using a  $\Sigma_s/\Sigma_T$  value of 0.987 (typical of ordinary concrete) were used to produce Figs. 2 and 3, in which the rate of saturation of the

---

2. S. Chandrasekhar, Radiative Transfer, p. 125, Oxford University Press (1950).

Table 2. Comparison of Monte Carlo Calculations of Differential Neutron Angular Albedos for Concrete\*with Exact Results of Chandrasekhar<sup>2</sup>

μ	dC/dΩ (neutrons·ster <sup>-1</sup> per incident neutron)							
	1 Scattering	Through 5 Scatterings	Through 10 Scatterings	Through 20 Scatterings	Through 50 Scatterings	Through 100 Scatterings	Through 200 Scatterings	Exact
1.0	3.92 x 10 <sup>-2</sup>	1.10 x 10 <sup>-1</sup>	1.46 x 10 <sup>-1</sup>	1.73 x 10 <sup>-1</sup>	1.93 x 10 <sup>-1</sup>	1.97 x 10 <sup>-1</sup>	1.98 x 10 <sup>-1</sup>	2.00 x 10 <sup>-1</sup>
0.9	3.72 x 10 <sup>-2</sup>	1.03 x 10 <sup>-1</sup>	1.35 x 10 <sup>-1</sup>	1.59 x 10 <sup>-1</sup>	1.76 x 10 <sup>-1</sup>	1.79 x 10 <sup>-1</sup>	1.80 x 10 <sup>-1</sup>	1.82 x 10 <sup>-1</sup>
0.8	3.50 x 10 <sup>-2</sup>	9.47 x 10 <sup>-2</sup>	1.22 x 10 <sup>-1</sup>	1.43 x 10 <sup>-1</sup>	1.58 x 10 <sup>-1</sup>	1.61 x 10 <sup>-1</sup>	1.61 x 10 <sup>-1</sup>	1.63 x 10 <sup>-1</sup>
0.7	3.24 x 10 <sup>-2</sup>	8.59 x 10 <sup>-2</sup>	1.10 x 10 <sup>-1</sup>	1.27 x 10 <sup>-1</sup>	1.39 x 10 <sup>-1</sup>	1.42 x 10 <sup>-1</sup>	1.42 x 10 <sup>-1</sup>	1.44 x 10 <sup>-1</sup>
0.6	2.96 x 10 <sup>-2</sup>	7.63 x 10 <sup>-2</sup>	9.63 x 10 <sup>-2</sup>	1.11 x 10 <sup>-1</sup>	1.20 x 10 <sup>-1</sup>	1.22 x 10 <sup>-1</sup>	1.23 x 10 <sup>-1</sup>	1.24 x 10 <sup>-1</sup>
0.4	2.27 x 10 <sup>-2</sup>	5.46 x 10 <sup>-2</sup>	6.67 x 10 <sup>-2</sup>	7.53 x 10 <sup>-2</sup>	8.09 x 10 <sup>-2</sup>	8.19 x 10 <sup>-2</sup>	8.21 x 10 <sup>-2</sup>	8.26 x 10 <sup>-2</sup>
0.3	1.85 x 10 <sup>-2</sup>	4.24 x 10 <sup>-2</sup>	5.08 x 10 <sup>-2</sup>	5.67 x 10 <sup>-2</sup>	6.06 x 10 <sup>-2</sup>	6.13 x 10 <sup>-2</sup>	6.14 x 10 <sup>-2</sup>	6.15 x 10 <sup>-2</sup>
0.2	1.34 x 10 <sup>-2</sup>	2.92 x 10 <sup>-2</sup>	3.43 x 10 <sup>-2</sup>	3.79 x 10 <sup>-2</sup>	4.02 x 10 <sup>-2</sup>	4.06 x 10 <sup>-2</sup>	4.07 x 10 <sup>-2</sup>	4.02 x 10 <sup>-2</sup>
0.1	7.35 x 10 <sup>-3</sup>	1.51 x 10 <sup>-2</sup>	1.73 x 10 <sup>-2</sup>	1.89 x 10 <sup>-2</sup>	1.99 x 10 <sup>-2</sup>	2.01 x 10 <sup>-2</sup>	2.01 x 10 <sup>-2</sup>	1.94 x 10 <sup>-2</sup>

\*Σ<sub>s</sub>/Σ<sub>T</sub> = 0.975; θ<sub>0</sub> = 0°.

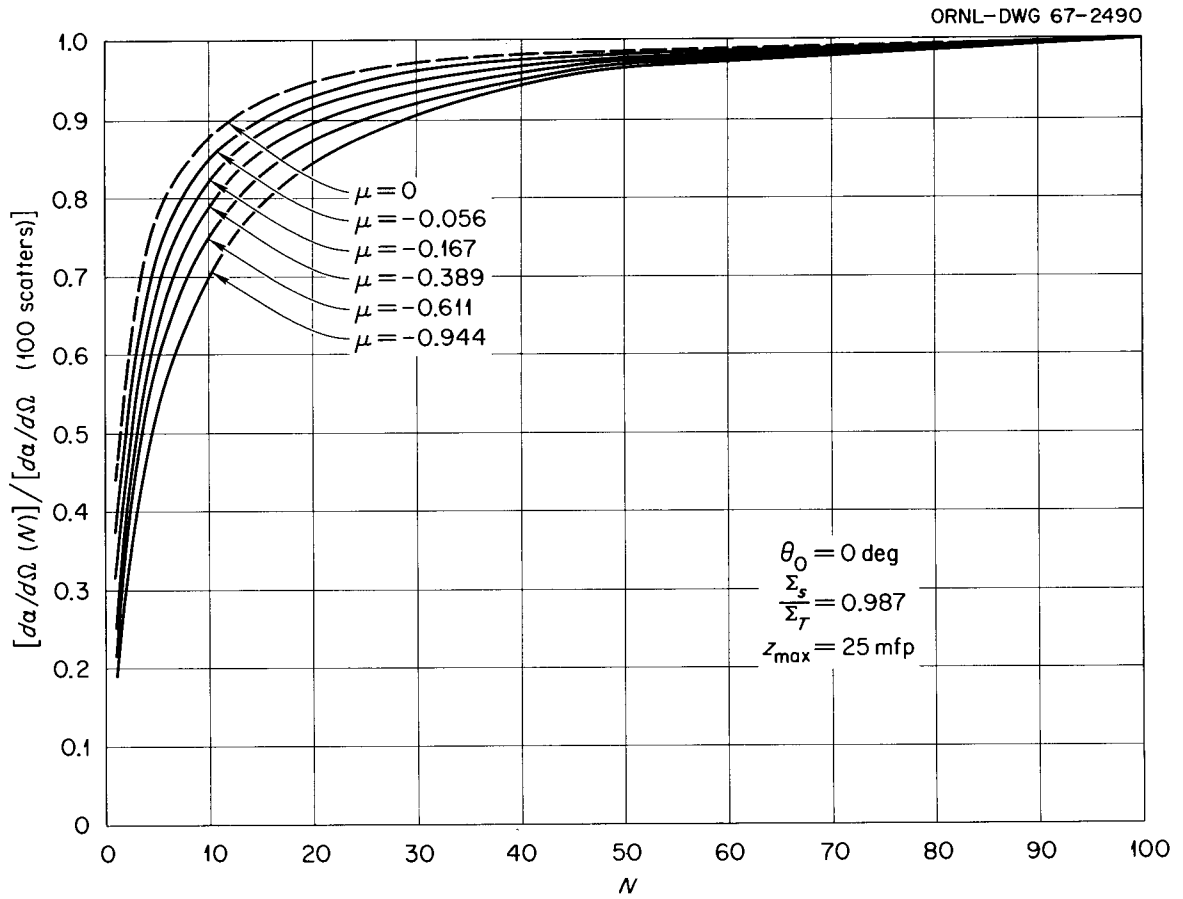


Fig. 2. Fraction of Total Differential Thermal-Neutron Angular Albedos as a Function of the Maximum Number of Allowed Neutron Scatterings  $N$ .

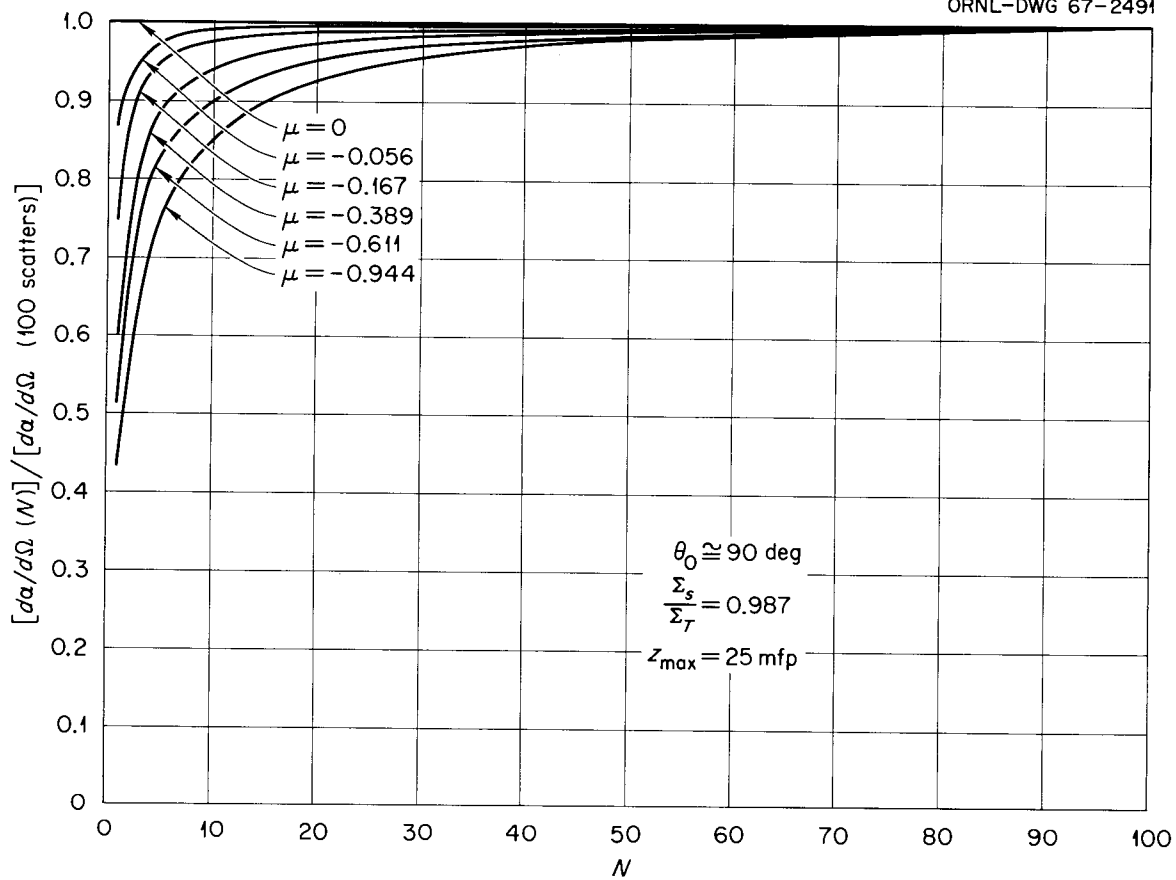


Fig. 3. Fraction of Total Differential Thermal-Neutron Angular Albedos as a Function of the Maximum Number of Allowed Neutron Scatterings  $N$ .

differential albedos are plotted as a function of the maximum order of allowed scattering,  $N$ , for essentially an infinitely thick slab. It is to be noted that the saturation rate is slowest for normal incidence, but that for 50 scatterings more than 95% of the differential albedo at any reflected angle has been attained. This is also verified from an inspection of Table 2.

The number of neutrons absorbed as a function of  $N$  and depth band,  $\Delta z$ , within a 25-mfp-thick slab is shown in Figs. 4 and 5 for the same incident conditions as in Figs. 2 and 3, respectively. The values calculated by Monte Carlo appear as histograms, and the saturated values are compared with results from a DTF one-energy group,  $S_{16}$  calculation. It is to be noted that the saturation rate is not a very sensitive function of the incident angle, but that the value of  $N$  required for saturation is a sensitive function of  $\Delta z$ . Thus, from Fig. 4, allowing up to 50 scatterings will saturate the captures in the depth region  $\Delta z = 0-1$  mfp, but 200 scatterings are required beyond a depth of 5 mfp. For a relatively thick slab (i.e.,  $z_{\max} > 5$  mfp), it is concluded therefore that allowing up to 200 scatterings is necessary to saturate the capture distribution.

A comparison of the differential angular albedos calculated by Monte Carlo for neutrons normally incident on an infinitely thick slab, having  $\Sigma_s/\Sigma_T = 0.987$ , with those obtained from a DTF one-energy group,  $S_{16}$  calculation is shown in Fig. 6. The number of allowed scatterings for the Monte Carlo calculation was 200, but 50 produced essentially the same result (see Fig. 2). Figure 7 shows a similar comparison of the distribution of captures within the semi-infinite slab, the number of allowed scatterings also being 200.

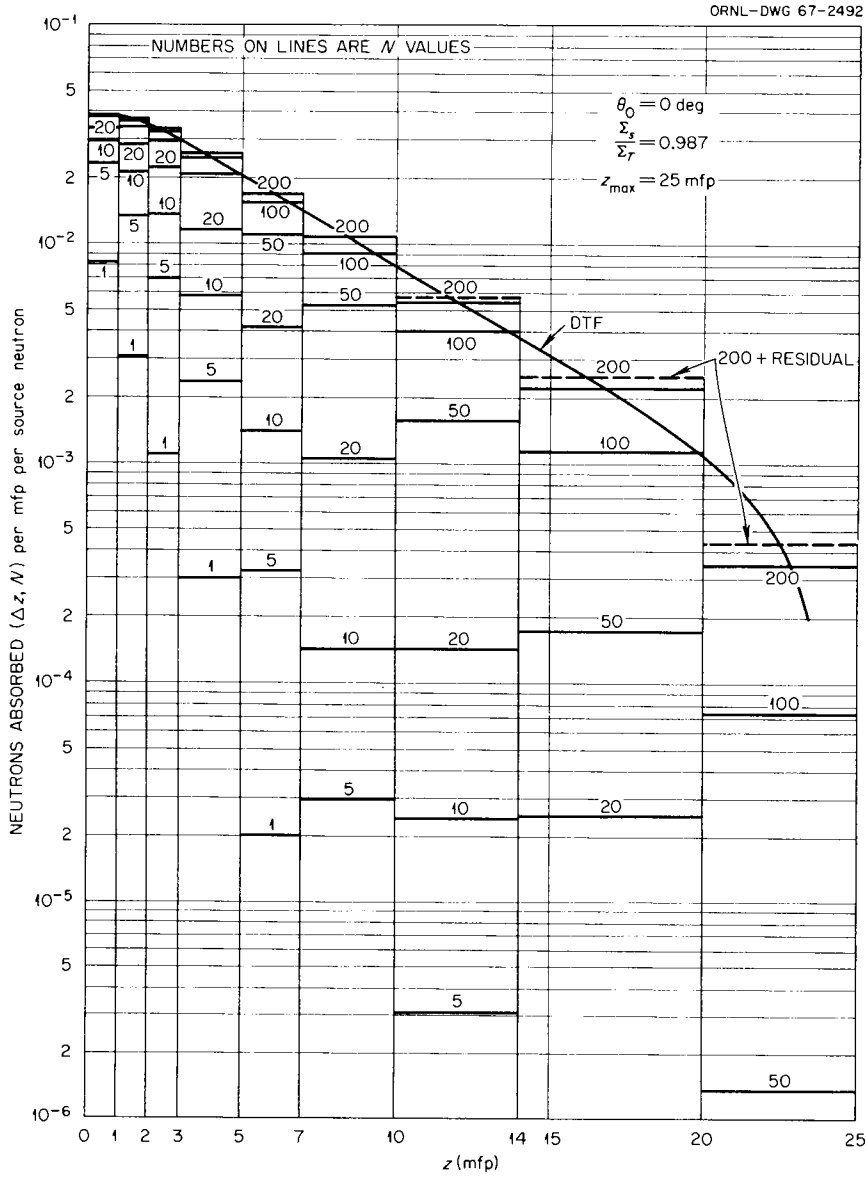


Fig. 4. Distribution of Captures in Concrete as a Function of the Maximum Number of Allowed Scatterings  $N$  for the Same Conditions Given in Fig. 2.

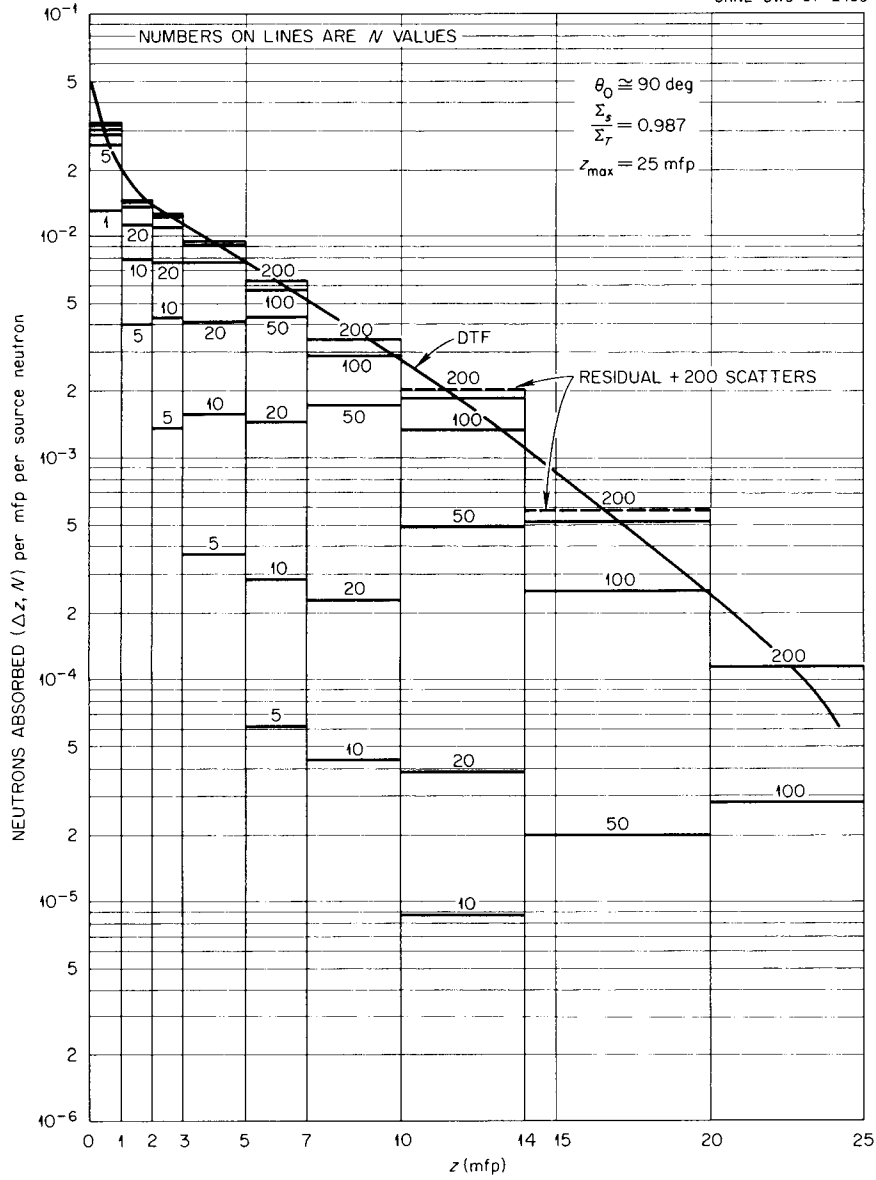


Fig. 5. Distribution of Captures in Concrete as a Function of the Maximum Number of Allowed Scatterings  $N$  for the Same Conditions Given in Fig. 3.

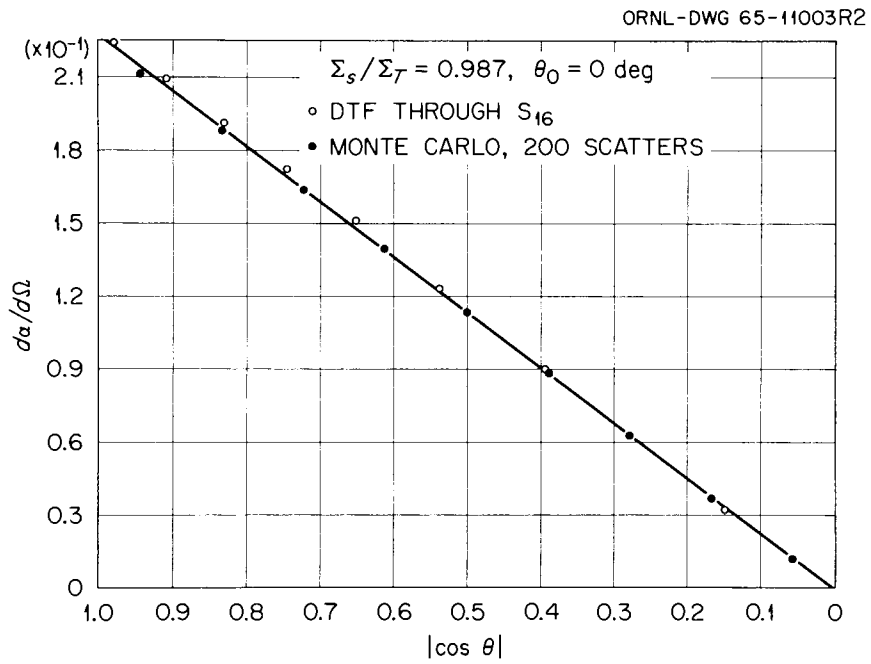


Fig. 6. Differential Thermal-Neutron Angular Albedos for a Semi-infinite Concrete Slab as a Function of the Cosine of the Polar Angle of Emission Assuming Isotropic Scattering and  $\Sigma_s/\Sigma_T = 0.987$ ; Comparison of Monte Carlo and DTF Calculations for Incident Angle of 0 deg.

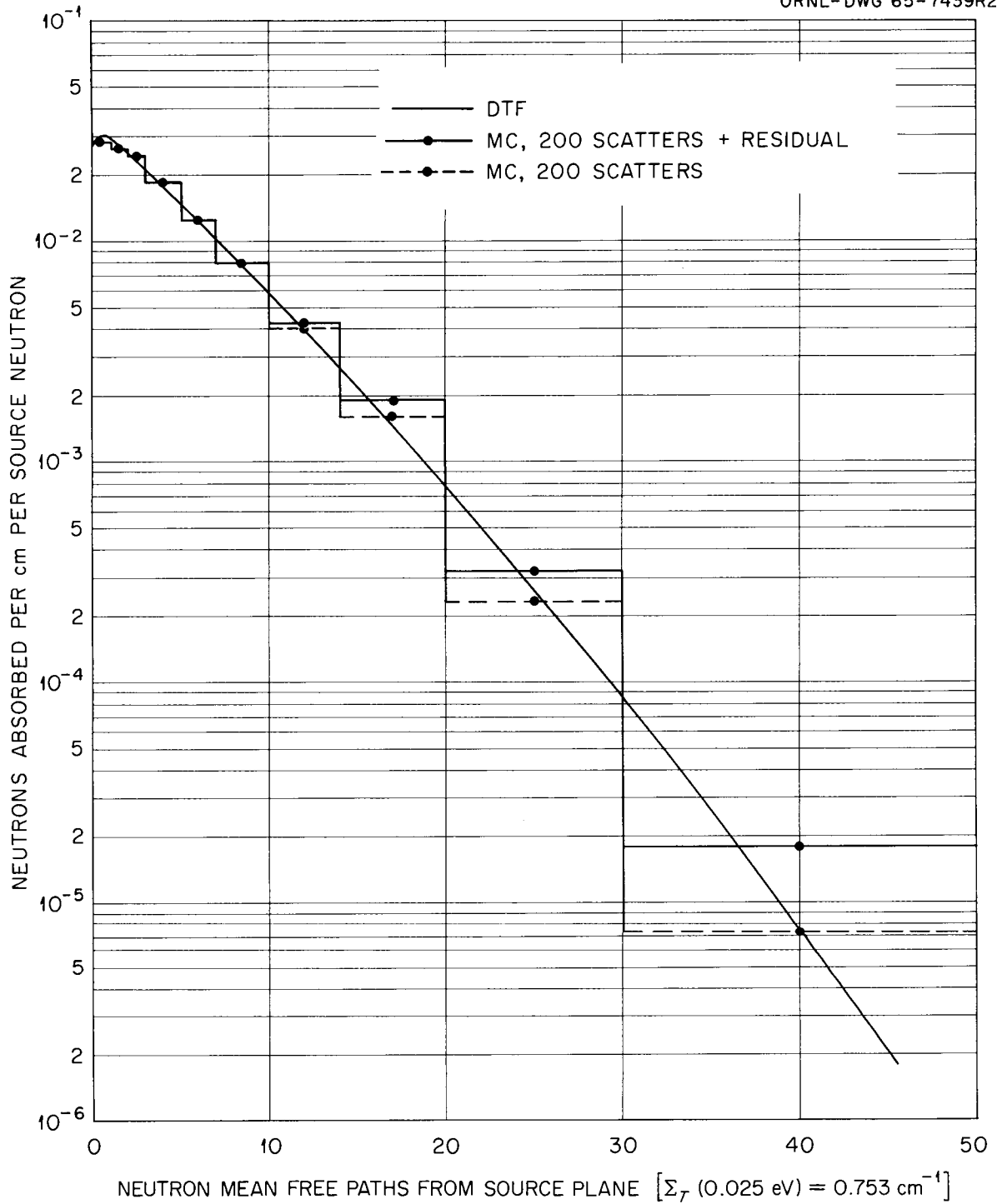


Fig. 7.. Distribution of Captures in Concrete for the Same Conditions given in Fig. 6: Comparison of Monte Carlo and DTF Calculations.

From inspection of the comparisons presented in Table 2 and Figs. 4-7, it can be concluded that the Monte Carlo method is quite feasible to employ in this type of calculation, but that a generous number of scatterings must be allowed in order to obtain good results. Although the computing times required for Monte Carlo calculations are somewhat longer than those of DTF calculations, the Monte Carlo procedure is more readily adaptable to geometric perturbations and to the inclusion of arbitrary anisotropic scattering functions. Furthermore, an azimuthal dependence of the angular albedos is easily calculated using a Monte Carlo procedure.

Correlated Monte Carlo calculations were also made as a function of slab thickness, in which the cumulative scores were tabulated for a history in boxes that only accepted a score if all the previous collisions occurred within a specified distance from the surface. Figures 8 and 9 show the nature of the saturation of the differential thermal-neutron albedo with slab thickness ( $z_{\max}$ ) for neutrons scattering 100 times or less. The incident neutrons are normal to the surface in Fig. 8 and almost parallel to the surface in Fig. 9. A slab 7 mean free paths thick ( $\sim 4$  in.) reflects at least 95% as many neutrons as are reflected by a slab of infinite thickness.

Figures 10 and 11 illustrate the dependence of the capture distributions on the thickness of the slab,  $z_{\max}$ , for the same incident conditions as Figs. 8 and 9, respectively, as calculated by Monte Carlo allowing up to 200 scatterings per neutron. Comparisons are made with DTF calculations for a thickness of 25 mfp. The effect of the rear boundary of the slab is of course greater the closer the depth region

ORNL-DWG 65-11001R

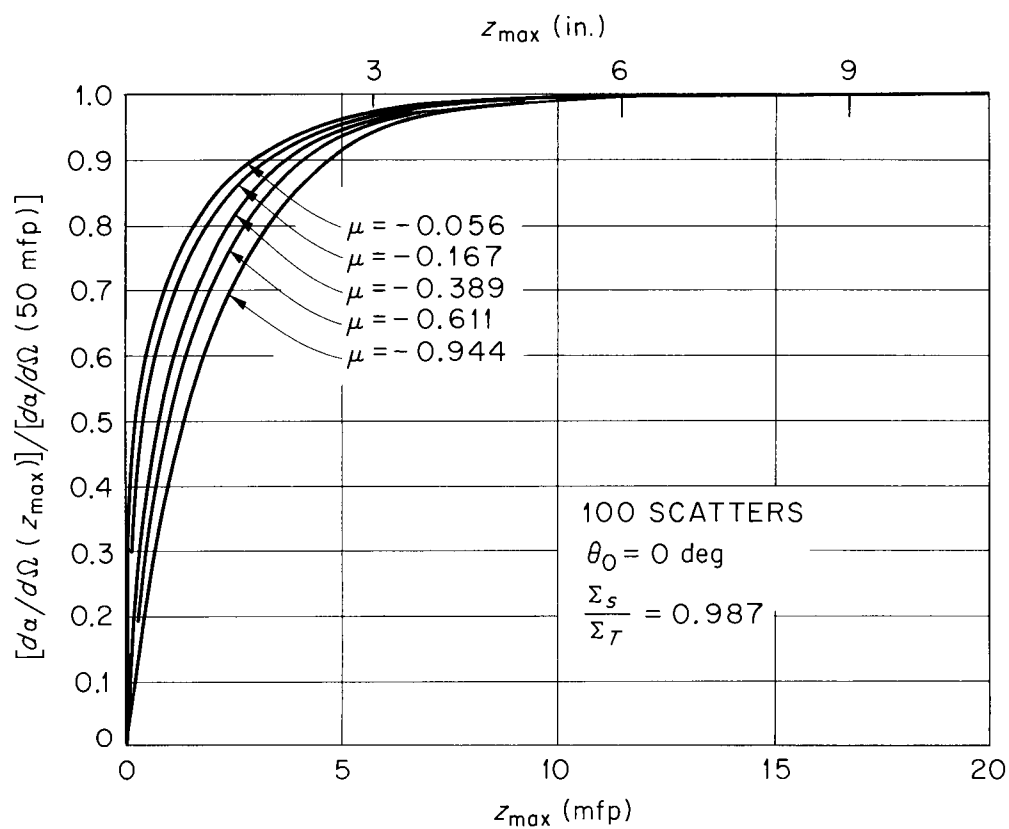


Fig. 8. Fraction of the Total Differential Thermal-Neutron Angular Albedos as a Function of Concrete Thickness.

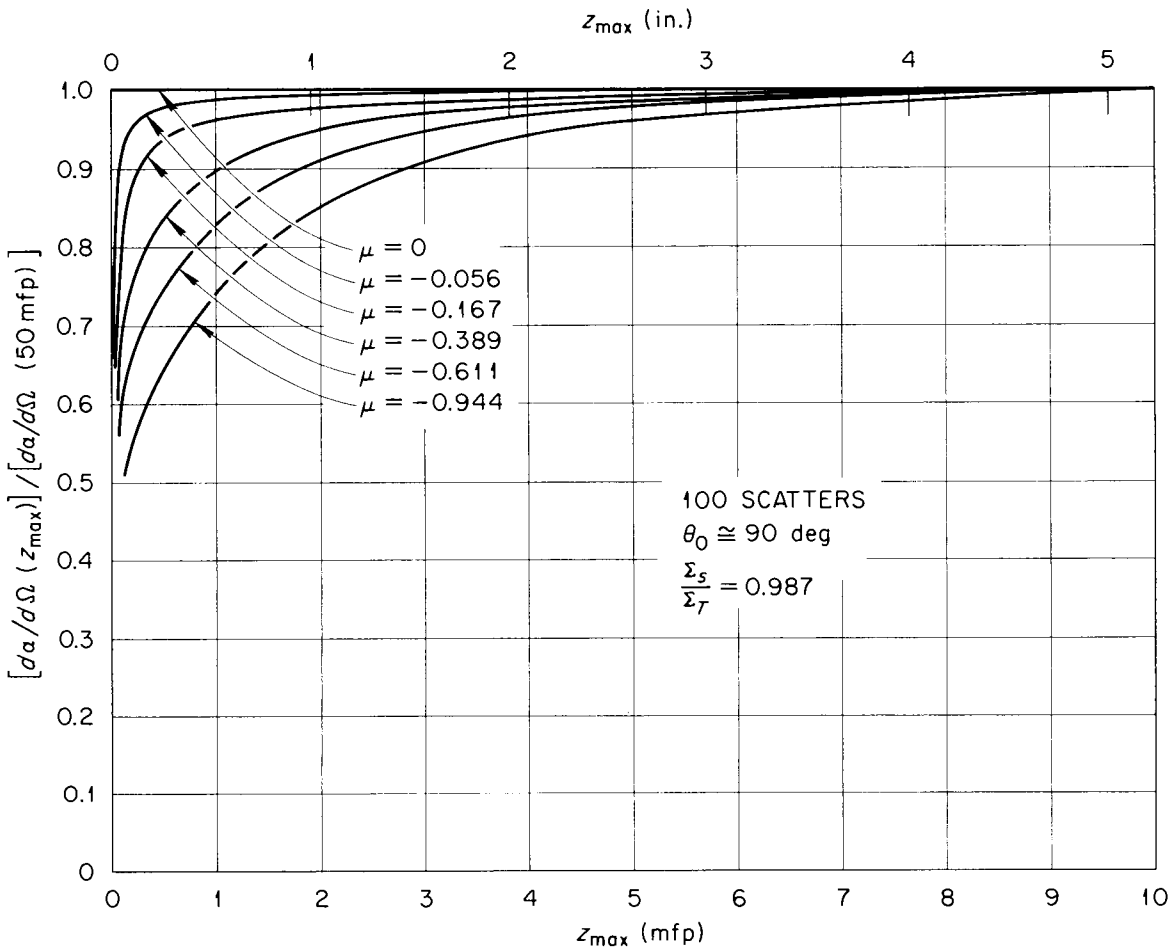


Fig. 9. Fraction of the Total Differential Thermal-Neutron Angular Albedos as a Function of Concrete Thickness.

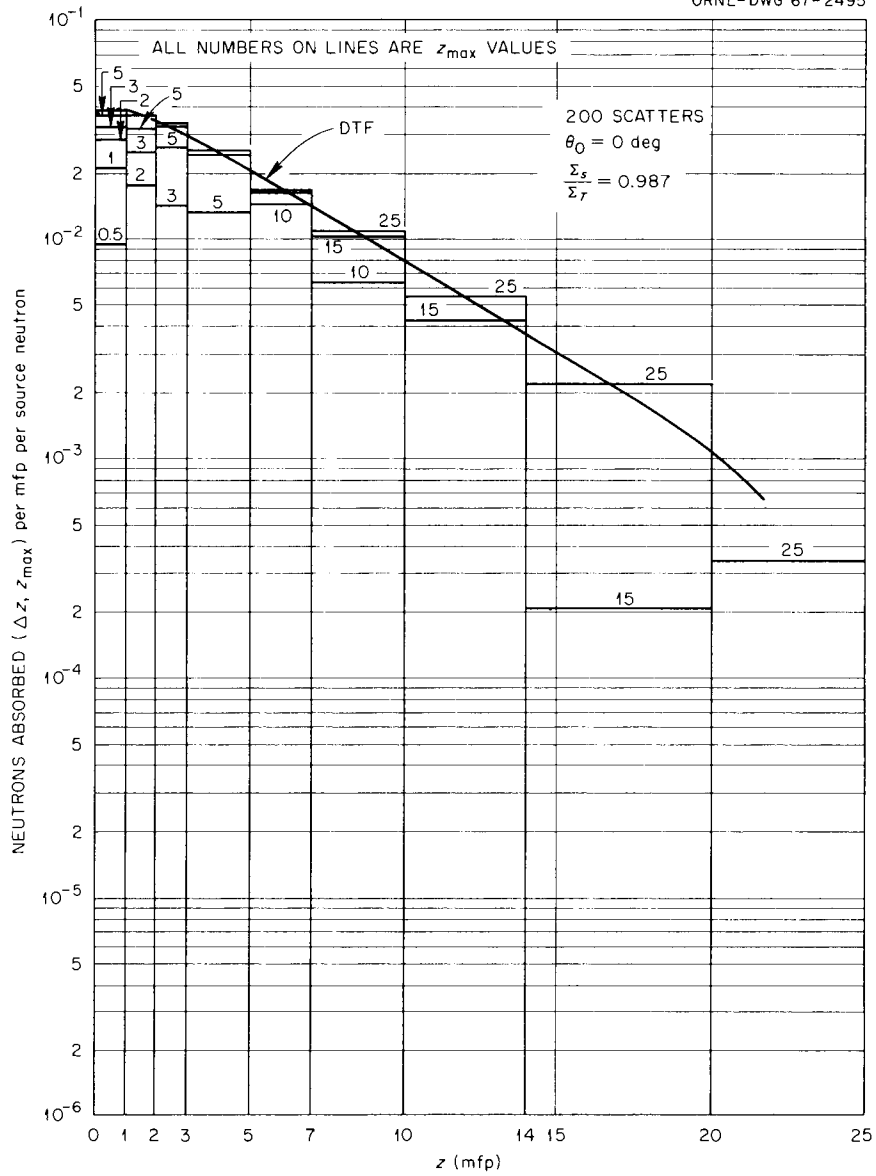


Fig. 10. Distribution of Captures in Concrete as a Function of Concrete Thickness ( $\theta_0 = 0 \text{ deg}$ ).

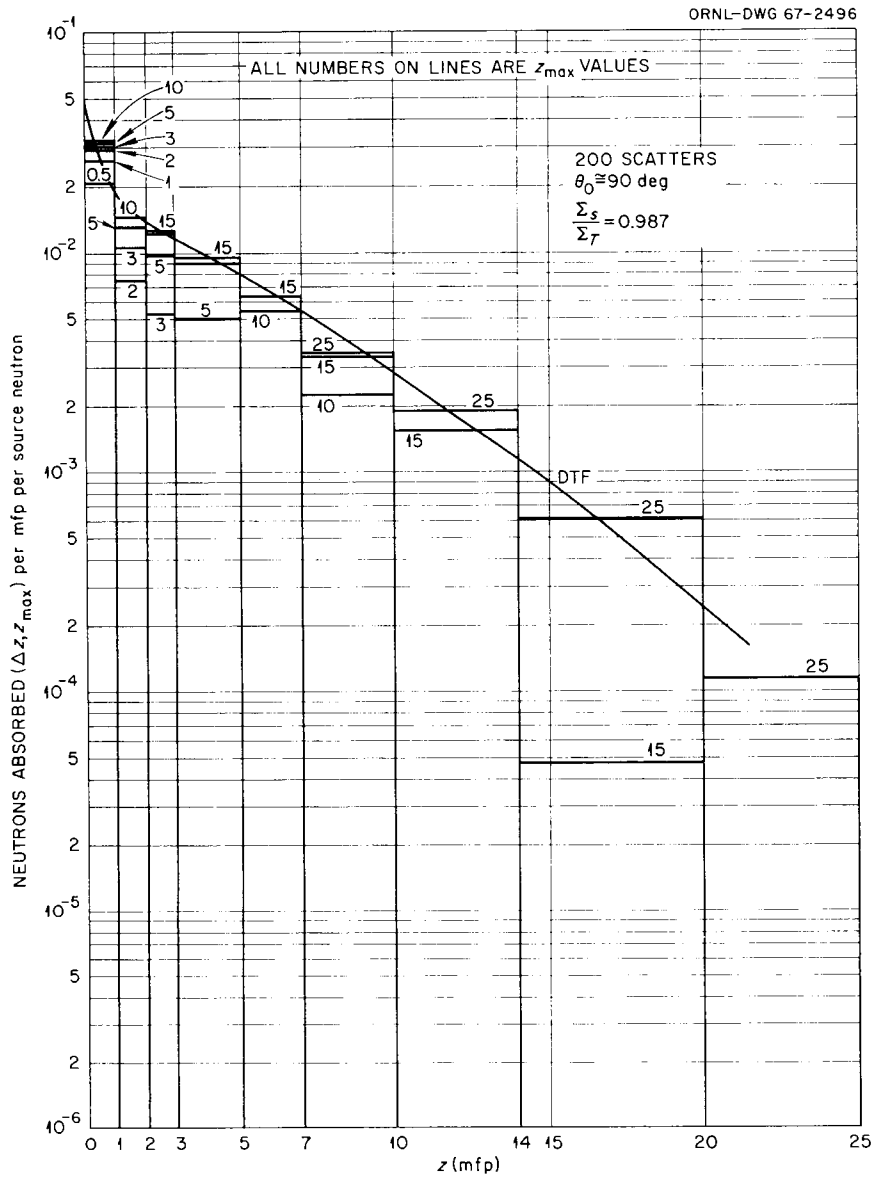


Fig. 11. Distribution of Captures in Concrete as a Function of Concrete Thickness ( $\theta_0 = 90$  deg).

lies to the boundary, but an inspection of these two figures indicates that boundary effects are significant only within depth regions lying within 5 mfp or so of the rear surface. Thus the depth distributions through 20 mfp or so presented for  $z_{\max} = 25$  mfp should be the same as those for a semi-infinite slab.

The capture distributions are significant only in that they give rise to capture gamma-ray dose rates, and the saturation of this dose rate with  $N$  and  $z_{\max}$  is illustrated in Figs. 12 and 13 for the case of normal incidence. Figure 12 shows the variation of the capture gamma-ray dose rate on the incident surface as a cumulative function of the maximum number of allowed scatterings for each thermal neutron, assuming 6 MeV as the average energy of the capture gamma rays. Approximately 100 scatterings must be followed to saturate the capture gamma-ray dose on the incident surface. Figure 13 shows the variation of the capture gamma-ray dose on the incident surface as a function of slab thickness for 200 neutron scatterings or less, still assuming a 6-MeV energy for the gamma rays. A slab 12 mean free paths thick to thermal neutrons ( $\sim 7$  in.) produces, on the incident surface, 95% or more of the capture gamma-ray dose generated from a slab of infinite thickness.

From the results of the calculations outlined above, it may be concluded that the 9-in.-thick concrete slab which was used in the experiments described below has essentially the same albedo characteristics as a semi-infinite medium.

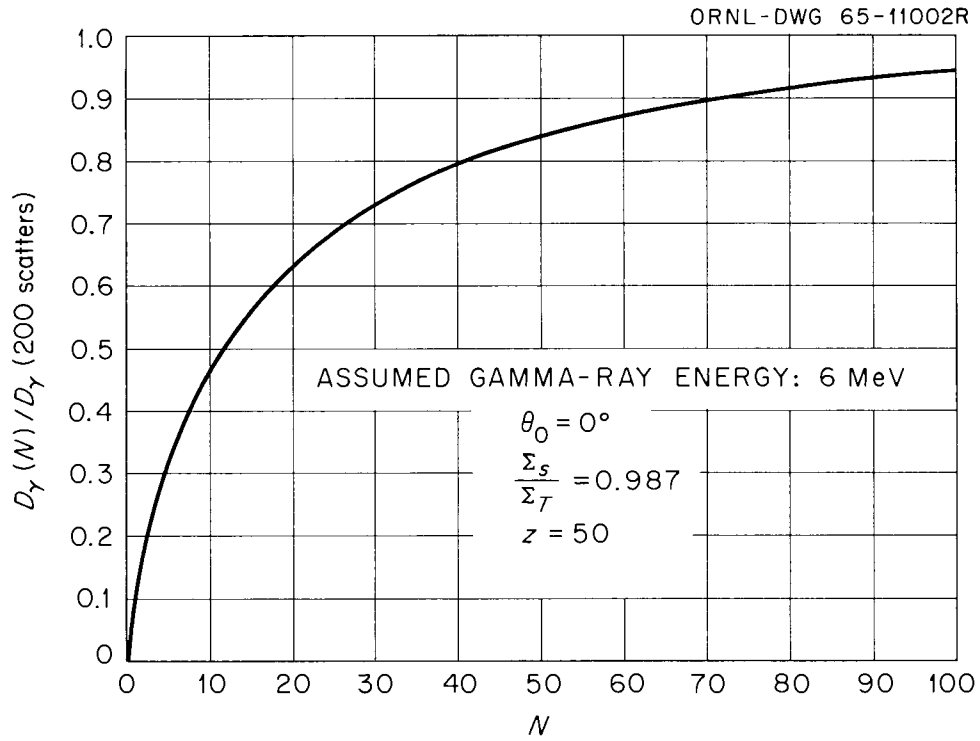


Fig. 12. Fraction of Total Capture Gamma-Ray Dose on Concrete Surface as a Function of the Maximum Number of Allowed Neutron Scatterings.

ORNL-DWG 65-11010

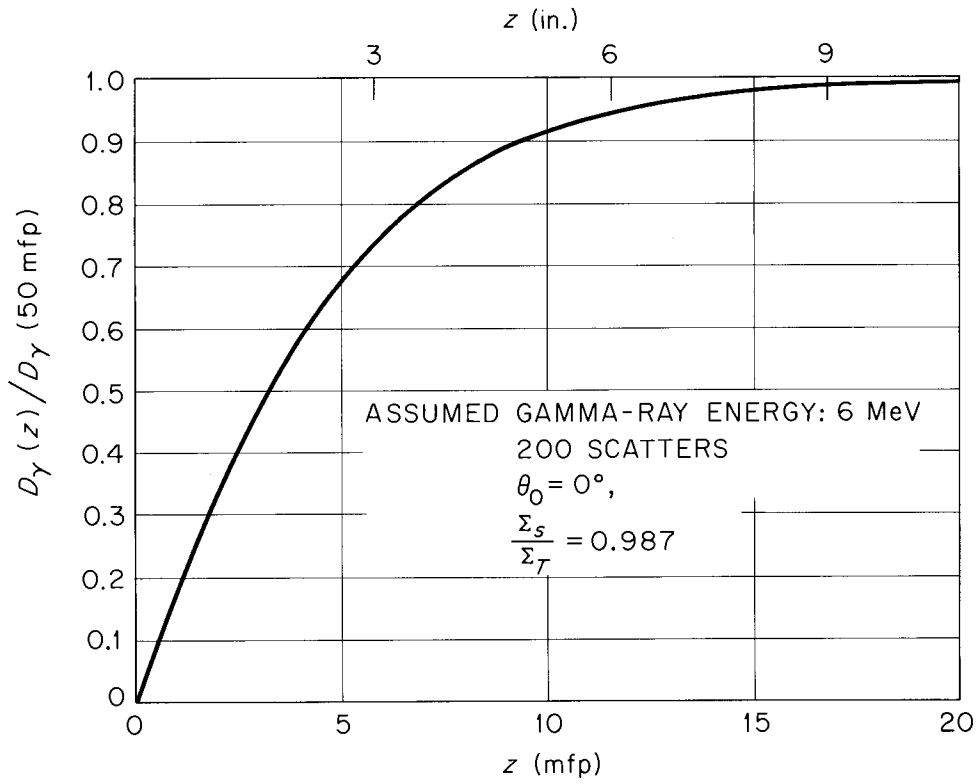


Fig. 13. Variation of Capture Gamma-Ray Dose on Surface of Concrete Slab with Slab Thickness.

### III. COMPARISON OF EXPERIMENT WITH CALCULATIONS INCLUDING PRESENCE OF THE IRON REINFORCING

Although the preceding calculations have shown the feasibility of using the Monte Carlo technique for solving thermal-neutron albedo and associated capture gamma-ray dose problems for weakly absorbing media, the accuracy of a one-velocity model in the calculation (i.e., ascribing energy-independent scattering and absorption laws to subcadmium neutrons) can best be ascertained by comparing the calculations with an experiment. The experimental data were obtained from a series of careful measurements performed at the TSF and utilizing a highly collimated neutron beam and a detector geometry analogous to that described previously for the fast-neutron albedo experiment.<sup>1</sup>

Figure 14 is a photograph of the experimental arrangement. A 9-in.-thick concrete slab having 1-in.-thick steel-reinforced regions centered at 1.75 and 7.25 in. from its front face was positioned in the neutron beam 8 ft from the end of the collimator. The 1/2-in.-diam reinforcing steel rods were placed in a grid type of arrangement of two groups of rods, one group perpendicular to the second group, in each of the two reinforcing regions. There were in all 14 rods in the region closest to the front face and they occupied approximately 4% of the first homogenized volume; there were 18 rods in the region closest to the back face and they occupied approximately 5% of the second homogenized volume. At this slab position more than 95% of the subcadmium neutrons in the beam were incident on the slab within 8 in. of the beam center line. The slab could be rotated about its horizontal axis, and the detector collimator, shown near the top of the photograph, could be rotated in the horizontal

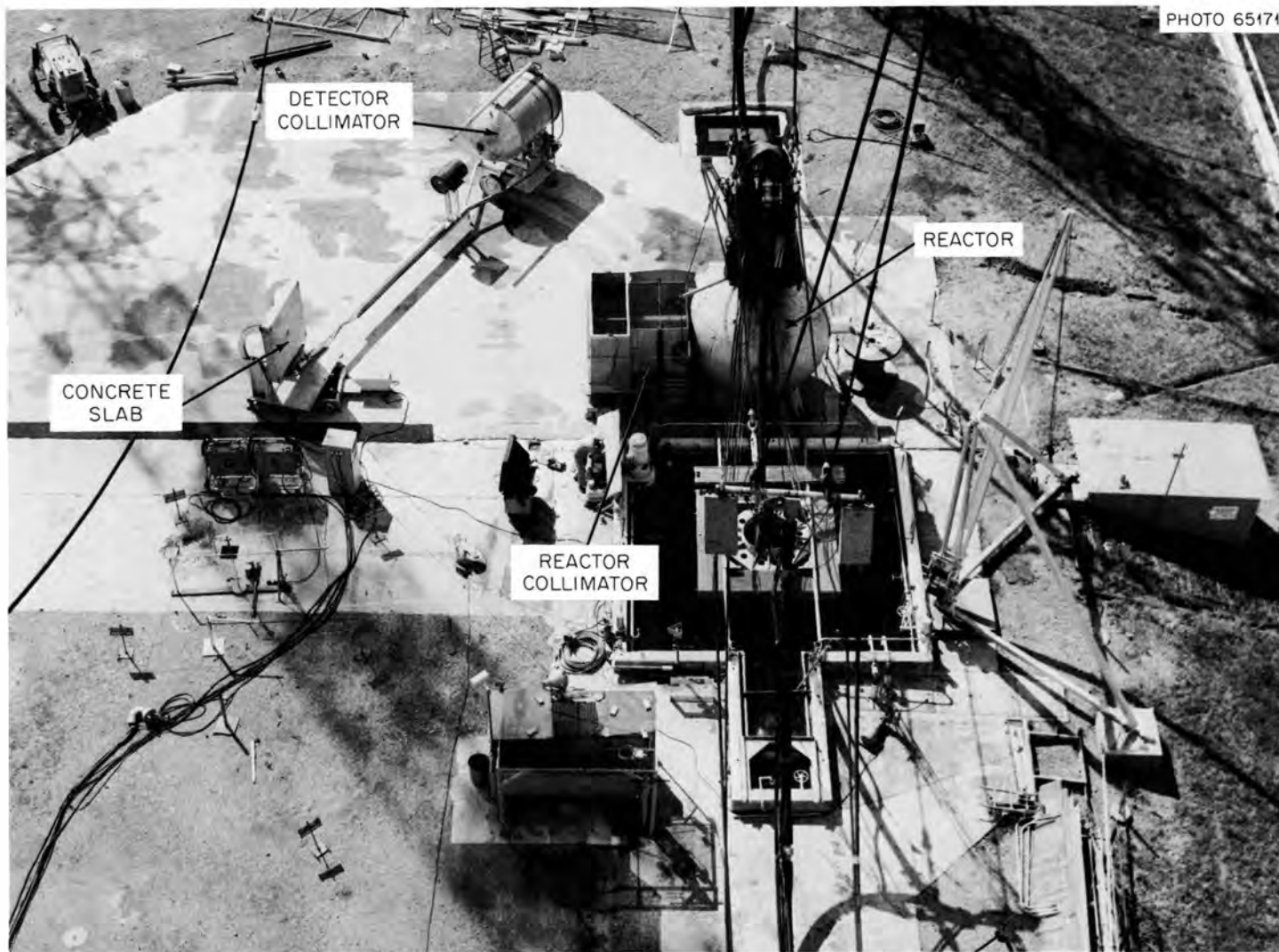


Fig. 14. Experimental Arrangement for Measuring Subcadmium Differential Neutron Albedos at Tower Shielding Facility.

plane at a fixed distance of 31 ft from the center of the slab. With the incident beam position fixed, almost the entire  $2\pi$  backscattered hemisphere could be scanned with this arrangement by moving the detector through a 160-deg arc in the horizontal plane and rotating the slab through 180 deg about a vertical axis and 90 deg about a horizontal axis. The angles which were measured in the experiment,  $\alpha$ ,  $\beta$ , and  $\gamma$ , are shown in Fig. 15, along with their functional relationships to  $\theta_0$ ,  $\theta$ , and  $\phi$ .

Subcadmium differential angular albedos were obtained for 72 different combinations of the incident angle and the reflected polar and azimuthal angles. Sixteen different measurements with a  $\text{BF}_3$  detector were necessary at each of the 72 combinations to effect a single measurement of the angular albedo. Cadmium-covered and bare-detector readings were taken for the cases of cadmium over the slab, cadmium over the reactor collimator, cadmium over both simultaneously, and both slab and collimator bare, for both foreground and background geometries.

Let the subscript 1 denote bare detector readings and the subscript 2 denote cadmium-covered detector readings, and

$A_n$  = detector reading with cadmium over the front face of the slab,

$B_n$  = detector reading with reactor collimator and slab bare,

$C_n$  = detector reading with cadmium over the reactor collimator,

$D_n$  = detector reading with cadmium over both the reactor collimator and front face of the slab,

$E_n, F_n, G_n, H_n$  = same as  $A_n, B_n, C_n, D_n$ , respectively, except that the slab has been rotated so that the line of sight from the detector to the slab is perpendicular to the slab normal.

ORNL-DWG 64-9856

$$\cos \gamma = -\cos \theta \cos \theta_0 - \sin \theta \sin \theta_0 \cos \phi$$

$$\cos \theta_0 = \cos \alpha \sin (\beta + \gamma)$$

$$\cos \alpha = -\cos \theta / \sin \beta$$

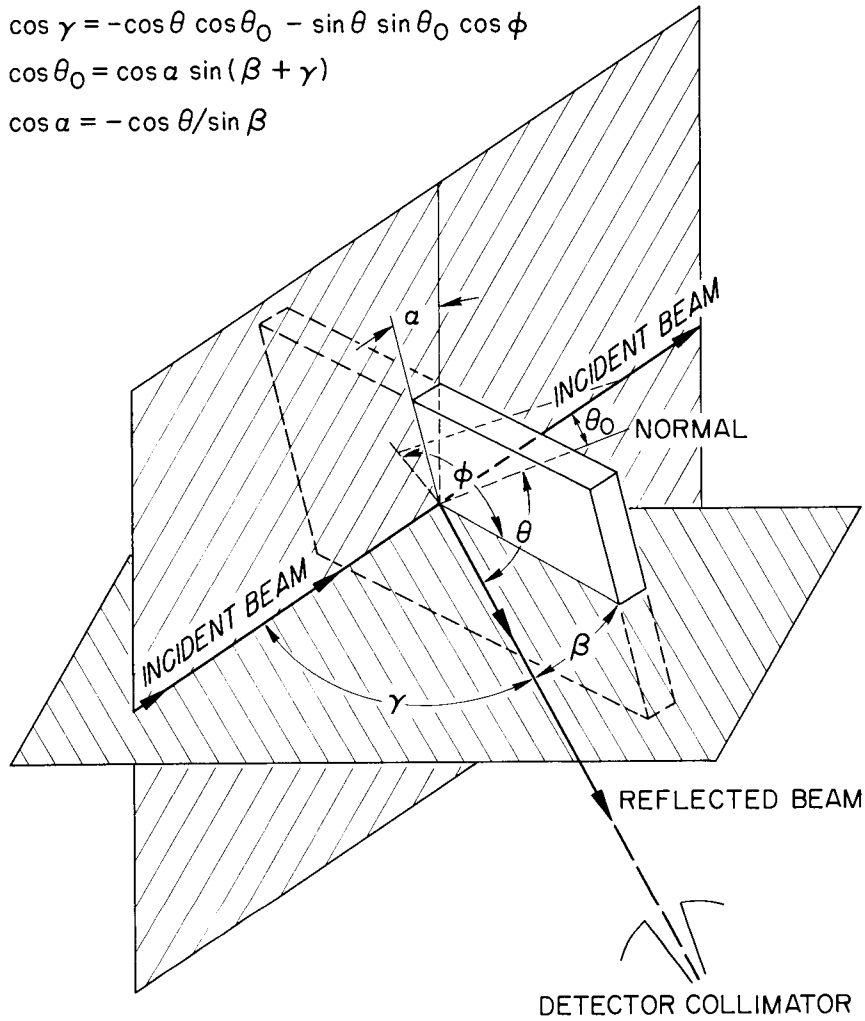


Fig. 15. The Experimental Angles,  $\alpha$ ,  $\beta$ , and  $\gamma$  and Their Functional Relationships to  $\theta_0$ ,  $\theta$ , and  $\phi$ .

Then

$$X = [(F_1 - F_2) - (E_1 - E_2)] - [(G_1 - G_2) - (H_1 - H_2)]$$

= contribution to detector reading from air scattering of incident subcadmium neutrons after slab reflection,

$$Y = [(C_1 - C_2) - (D_1 - D_2)] - [(G_1 - G_2) - (H_1 - H_2)]$$

= contribution to detector reading from subcadmium neutrons generated within the slab from incident episcadmium neutrons, and

$$Z = [(B_1 - B_2) - (A_1 - A_2)] - [(F_1 - F_2) - (E_1 - E_2)] - Y$$

= contribution to detector reading from subcadmium neutrons due to slab reflection of incident subcadmium neutrons.

The component Z was corrected for air attenuation and the inverse square effect to the detector and then divided by the incident subcadmium current integrated over the surface of the slab to determine the thermal differential angular albedo at the particular angles measured:

$$\begin{aligned} d\alpha/d\Omega(\theta_0, \theta, \phi) &= Z (\text{counts}\cdot\text{min}^{-1}\cdot\text{W}^{-1}) \times 4.30 \times 10^{-3} (\text{neut}\cdot\text{cm}^{-2}\cdot\text{sec}^{-1} / \\ &\quad \text{count}\cdot\text{min}^{-1}) \times \frac{(31 \times 30.5)^2 \times \exp(31/70)}{1.53 \times 10^3 \text{ neut}\cdot\text{sec}^{-1}\cdot\text{W}^{-1}} \\ &= 3.92 Z (\text{counts}\cdot\text{min}^{-1}\cdot\text{W}^{-1}) \end{aligned}$$

For the calculations, the experimental slab was divided into five regions, having  $\Sigma_s/\Sigma_T$  values of 0.987, 0.978, 0.987, 0.978, and 0.987 (0.025-eV values), the lower values representing the steel-reinforced regions. The incident neutrons were followed for 200 scatterings, with two scattering laws being assumed: (1) isotropic scattering in the laboratory system for all elements; that is, the hydrogen is completely

bound to the oxygen in the case of water, and the small anisotropy in the scattering cross sections of the other elements is neglected; and (2) anisotropic water scattering, using a scattering law deduced from the results of experiments by Greenspan and Baksys,<sup>3</sup> at an energy of 0.0358 eV, together with isotropic laboratory scattering for nonwater oxygen, calcium, etc. The shape of the anisotropic differential scattering cross section for water is shown in Fig. 16. In both cases (1) and (2), the total cross section for water was normalized to the 0.025-eV value of 105 barns.<sup>4</sup> Ten problems were computed following 2000 histories in each problem for five angles of incidence and two scattering laws.

In addition to the thermal-neutron differential angular albedos, the number of thermal-neutron captures as a function of depth within the slab was also calculated. These values appear in the Appendix. These numbers were multiplied by the number of gamma rays emitted per capture as a function of region and gamma-ray energy,<sup>5</sup> and the resulting gamma-ray differential angular current in dose rate units escaping the front surface was calculated by another Monte Carlo program.<sup>6</sup>

A comparison of the measurements with the two Monte Carlo calculations is shown in Figs. 17-21 and Tables 3-6. It is to be observed that a definite azimuthal variation is found experimentally, although it is not nearly as large as that found for the fast-neutron dose,<sup>1</sup> and that using the anisotropic scattering cross-section shape deduced from the

3. H. Greenspan and I. G. Baksys, Differential Scattering Cross Sections for Slow Neutrons in H<sub>2</sub>O, Addenda, Newsletter No. 9, Argonne National Laboratory (March 1963).
4. D. J. Hughes and R. S. Carter, Neutron Cross Sections, BNL-325, Brookhaven National Laboratory (1955).
5. E. P. Blizard and L. S. Abbott, eds., Reactor Handbook 2nd Ed., Vol. III, Part B, "Shielding," pp 45-46, Interscience Publishers, New York (1962).
6. S. K. Penny, D. K. Trubey, and M. B. Emmett, OGRE, A Monte Carlo System for the Study of Gamma-Ray Transport, ORNL-3805, Oak Ridge National Laboratory (1966).

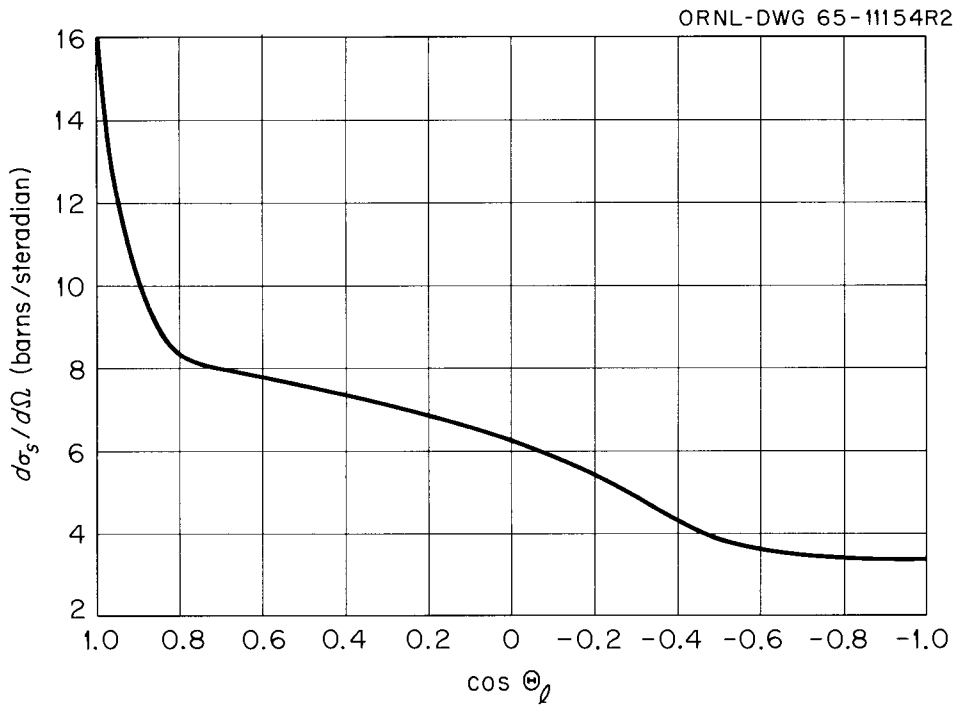


Fig. 16. Differential Scattering Cross Section for Water as a Function of Cosine of the Angle of Scatter in the Laboratory System. Derived from the measurements of Greenspan and Baksys at 293°K and 0.0358 eV.

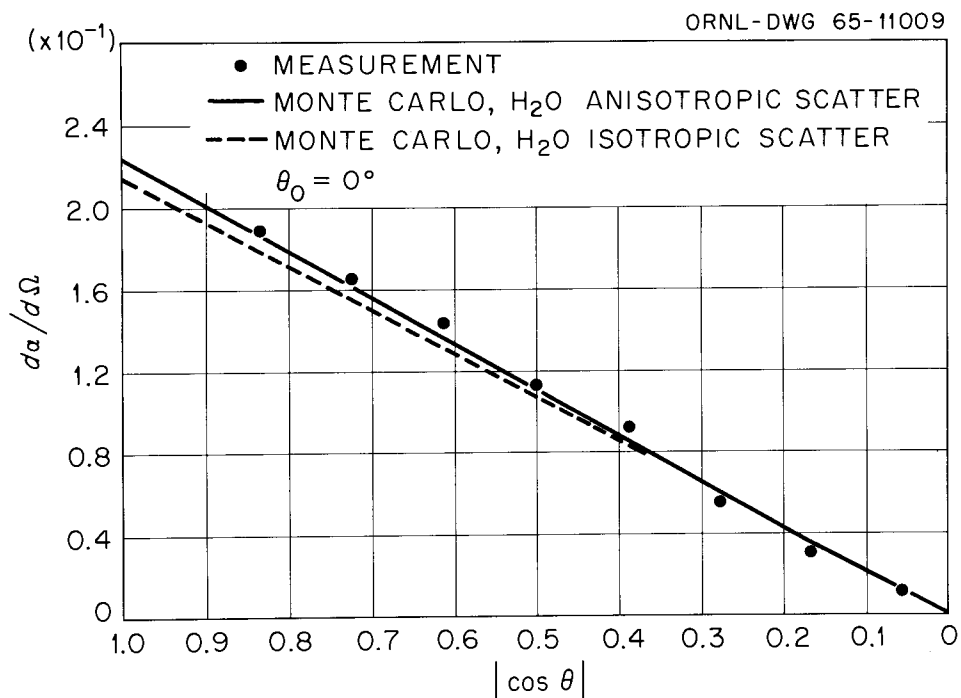


Fig. 17. Subcadmium Neutron Differential Albedo for Reinforced Concrete as a Function of the Cosine of the Polar Angle of Emission ( $\theta_0 = 0$  deg).

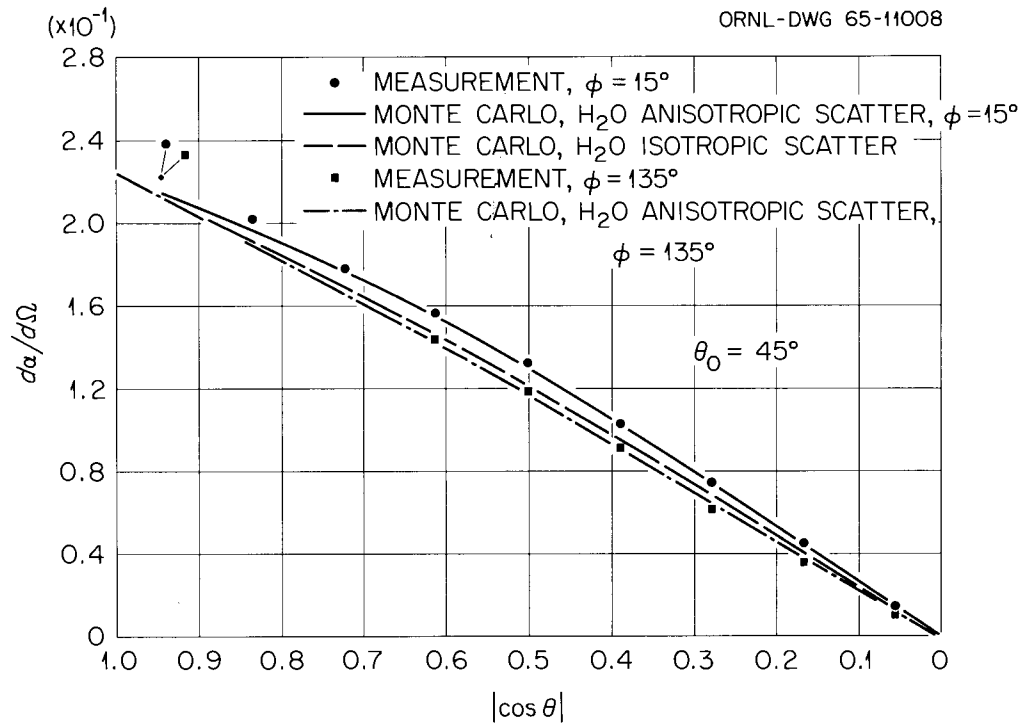


Fig. 18. Subcadmium Neutron Differential Albedo for Reinforced Concrete as a Function of the Cosine of the Polar Angle of Emission ( $\theta_0 = 45$  deg).

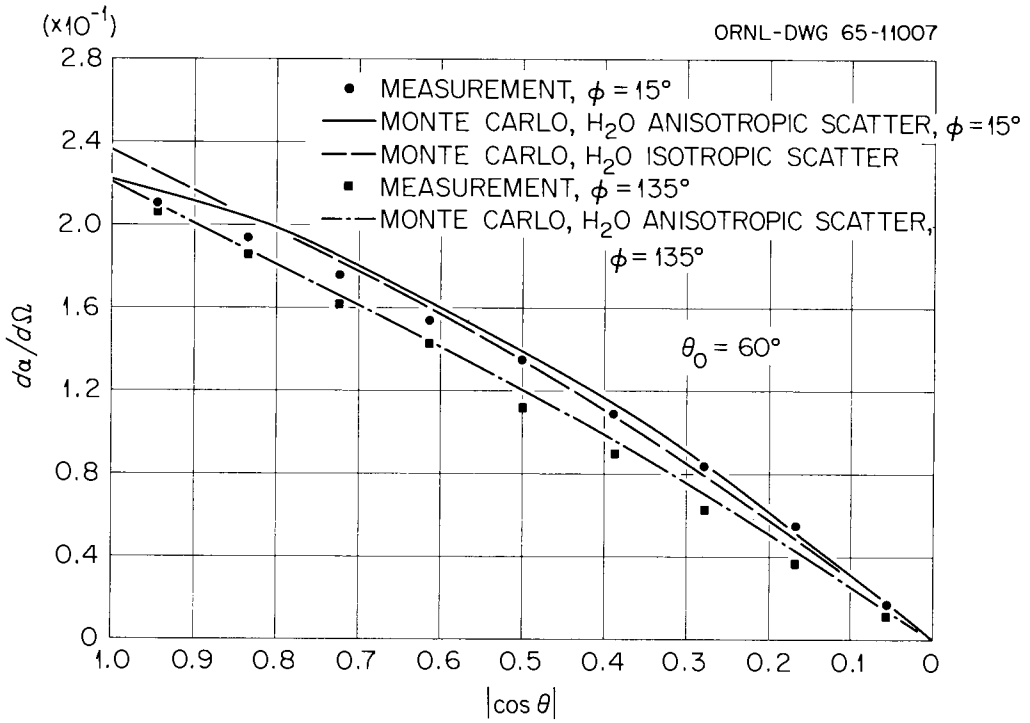


Fig. 19. Subcadmium Neutron Differential Albedo for Reinforced Concrete as a Function of the Cosine of the Polar Angle of Emission ( $\theta_0 = 60$  deg).

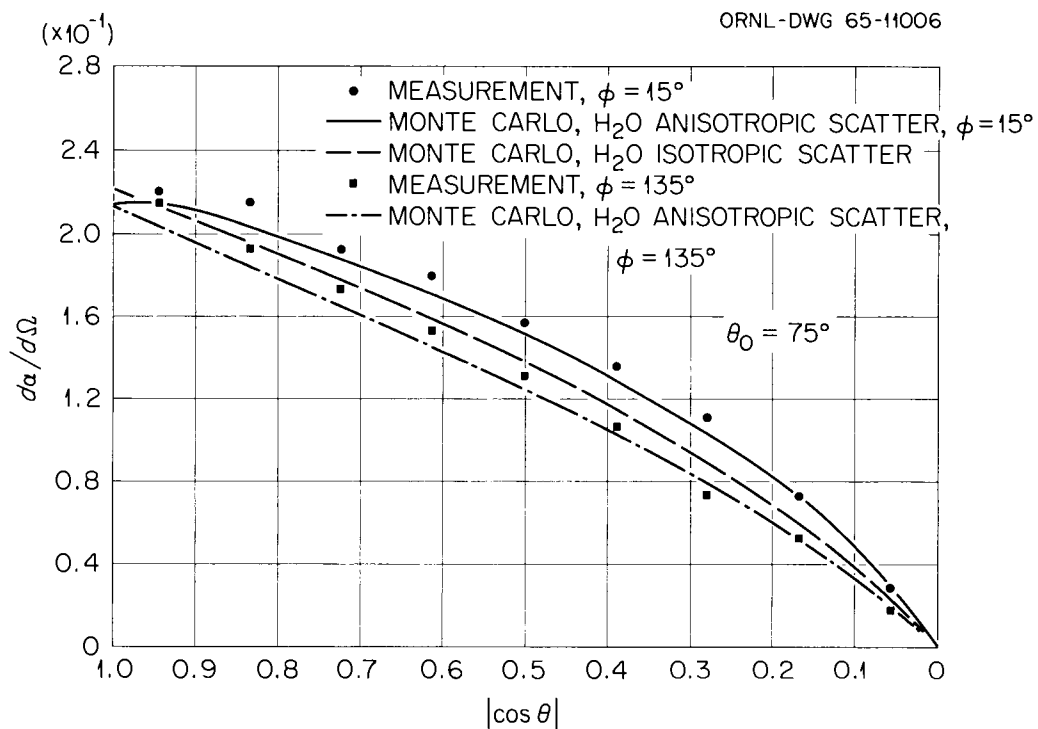


Fig. 20. Subcadmium Neutron Differential Albedo for Reinforced Concrete as a Function of the Azimuthal Angle of Emission (Incident Angle =  $75^\circ$ ).

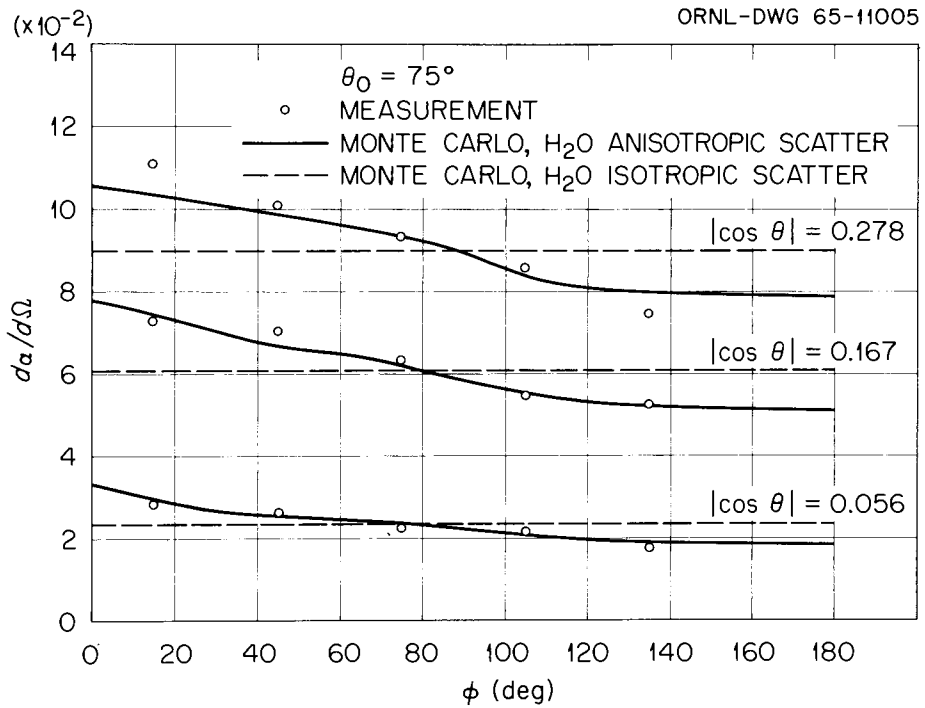


Fig. 21. Subcadmium Neutron Differential Albedo for Reinforced Concrete as a Function of the Cosine of the Azimuthal Angle of Emission (Incident Angle =  $75^\circ$ ).

Table 3. Comparison of Calculated Values of  $d\alpha/d\Omega$  with Experiment for  $\theta_0 = 0$  deg

$ \cos\theta $	$\frac{z}{\text{(cts}\cdot\text{min}^{-1}\cdot\text{W}^{-1})}$	$d\alpha/d\Omega$ (neutrons $\cdot$ ster $^{-1}$ per source neutron)		
		Measured	Calculated	
			Isotropic Scattering	Anisotropic Water Scattering <sup>a</sup>
0.944			$2.02 \times 10^{-1}$	$2.12 \times 10^{-1}$
0.833	$4.83 \times 10^{-2}$	$1.89 \times 10^{-1}$	$1.79 \times 10^{-1}$	$1.87 \times 10^{-1}$
0.722	$4.20 \times 10^{-2}$	$1.65 \times 10^{-1}$	$1.57 \times 10^{-1}$	$1.62 \times 10^{-1}$
0.611	$3.68 \times 10^{-2}$	$1.44 \times 10^{-1}$	$1.33 \times 10^{-1}$	$1.36 \times 10^{-1}$
0.5	$2.88 \times 10^{-2}$	$1.13 \times 10^{-1}$	$1.09 \times 10^{-1}$	$1.10 \times 10^{-1}$
0.389	$2.35 \times 10^{-2}$	$9.21 \times 10^{-2}$	$8.46 \times 10^{-2}$	$8.52 \times 10^{-2}$
0.278	$1.42 \times 10^{-2}$	$5.57 \times 10^{-2}$	$5.96 \times 10^{-2}$	$5.98 \times 10^{-2}$
0.167	$7.88 \times 10^{-3}$	$3.09 \times 10^{-2}$	$3.46 \times 10^{-2}$	$3.48 \times 10^{-2}$
0.056	$2.96 \times 10^{-3}$	$1.16 \times 10^{-2}$	$1.08 \times 10^{-2}$	$1.07 \times 10^{-2}$

a. Average of two runs.

Table 4. Comparison of Calculated Values of  $d\alpha/d\Omega$  with Experiment for  $\theta_0 = 45$  deg

cos $\theta$	$\phi$ (deg)	$z$ (cts·min <sup>-1</sup> ·W <sup>-1</sup> )	$d\alpha/d\Omega$ (neutrons·ster <sup>-1</sup> per source neutron)		
			Measured	Calculated	
				Isotropic Scattering <sup>a</sup>	Anisotropic Water Scattering
0.944	15	5.67 x 10 <sup>-2</sup>	2.22 x 10 <sup>-1</sup>	2.13 x 10 <sup>-1</sup>	2.14 x 10 <sup>-1</sup>
	45				2.12 x 10 <sup>-1</sup>
	75				2.12 x 10 <sup>-1</sup>
	105				2.12 x 10 <sup>-1</sup>
	135				2.12 x 10 <sup>-1</sup>
0.833	15	5.69 x 10 <sup>-2</sup>	2.23 x 10 <sup>-1</sup>	1.92 x 10 <sup>-1</sup>	2.11 x 10 <sup>-1</sup>
	45				1.97 x 10 <sup>-1</sup>
	75				1.94 x 10 <sup>-1</sup>
	105				1.90 x 10 <sup>-1</sup>
	135				1.89 x 10 <sup>-1</sup>
0.722	15	4.54 x 10 <sup>-2</sup>	1.78 x 10 <sup>-1</sup>	1.69 x 10 <sup>-1</sup>	1.89 x 10 <sup>-1</sup>
	45				1.78 x 10 <sup>-1</sup>
	75				1.74 x 10 <sup>-1</sup>
	105				1.69 x 10 <sup>-1</sup>
	135				1.67 x 10 <sup>-1</sup>
0.611	15	3.97 x 10 <sup>-2</sup>	1.56 x 10 <sup>-1</sup>	1.46 x 10 <sup>-1</sup>	1.66 x 10 <sup>-1</sup>
	45				1.56 x 10 <sup>-1</sup>
	75				1.52 x 10 <sup>-1</sup>
	105				1.47 x 10 <sup>-1</sup>
	135				1.42 x 10 <sup>-1</sup>
0.5	15	3.68 x 10 <sup>-2</sup>	1.44 x 10 <sup>-1</sup>	1.22 x 10 <sup>-1</sup>	1.42 x 10 <sup>-1</sup>
	45				1.42 x 10 <sup>-1</sup>
	75				1.31 x 10 <sup>-1</sup>
	105				1.29 x 10 <sup>-1</sup>
	135				1.23 x 10 <sup>-1</sup>
0.389	15	3.38 x 10 <sup>-2</sup>	1.32 x 10 <sup>-1</sup>	9.61 x 10 <sup>-2</sup>	1.18 x 10 <sup>-1</sup>
	45				1.17 x 10 <sup>-1</sup>
	75				1.17 x 10 <sup>-1</sup>
	105				1.04 x 10 <sup>-1</sup>
	135				1.02 x 10 <sup>-1</sup>
0.278	15	2.63 x 10 <sup>-2</sup>	1.03 x 10 <sup>-1</sup>	6.95 x 10 <sup>-2</sup>	9.80 x 10 <sup>-2</sup>
	45				9.24 x 10 <sup>-2</sup>
	75				9.11 x 10 <sup>-2</sup>
	105				9.09 x 10 <sup>-2</sup>
	135				9.13 x 10 <sup>-2</sup>
	15	2.33 x 10 <sup>-2</sup>	9.13 x 10 <sup>-2</sup>		7.56 x 10 <sup>-2</sup>
	45				7.42 x 10 <sup>-2</sup>
	75				7.12 x 10 <sup>-2</sup>
	105				6.65 x 10 <sup>-2</sup>
	135				6.46 x 10 <sup>-2</sup>
	15	1.89 x 10 <sup>-2</sup>	7.41 x 10 <sup>-2</sup>	6.95 x 10 <sup>-2</sup>	6.44 x 10 <sup>-2</sup>
	45				
	75				
	105	1.58 x 10 <sup>-2</sup>	6.19 x 10 <sup>-2</sup>		6.65 x 10 <sup>-2</sup>
	135				
	165				

Table 4 (contd.)

cosθ	φ (deg)	z (cts.min <sup>-1</sup> .W <sup>-1</sup> )	dα/dΩ (neutrons.ster <sup>-1</sup> per source neutron)		
			Measured	Calculated	
				Isotropic Scattering <sup>a</sup>	Anisotropic Water Scattering
0.167	15	1.14 x 10 <sup>-2</sup>	4.47 x 10 <sup>-2</sup>	4.19 x 10 <sup>-2</sup>	4.57 x 10 <sup>-2</sup>
	45				4.47 x 10 <sup>-2</sup>
	75				4.29 x 10 <sup>-2</sup>
	105	9.16 x 10 <sup>-3</sup>			3.97 x 10 <sup>-2</sup>
	135				3.78 x 10 <sup>-2</sup>
	165				3.76 x 10 <sup>-2</sup>
0.056	15	3.72 x 10 <sup>-3</sup>	1.46 x 10 <sup>-2</sup>	1.40 x 10 <sup>-2</sup>	1.49 x 10 <sup>-2</sup>
	45				1.45 x 10 <sup>-2</sup>
	75				1.39 x 10 <sup>-2</sup>
	105	2.86 x 10 <sup>-3</sup>			1.27 x 10 <sup>-2</sup>
	135				1.18 x 10 <sup>-2</sup>
	165				1.18 x 10 <sup>-2</sup>

a. There is no azimuthal dependence for the calculation assuming isotropic scattering.

Table 5. Comparison of Calculated Values of  $d\alpha/d\Omega$  with Experiment for  $\theta_0 = 60$  deg

$ \cos\theta $	$\phi$ (deg)	$z$ (cts·min <sup>-1</sup> ·W <sup>-1</sup> )	$d\alpha/d\Omega$ (neutrons·ster <sup>-1</sup> per source neutron)		
			Measured	Calculated	
				Isotropic Scattering	Anisotropic Water Scattering <sup>a</sup>
0.944	15	$5.36 \times 10^{-2}$	$2.10 \times 10^{-1}$	$2.25 \times 10^{-1}$	$2.18 \times 10^{-1}$
	45				$2.15 \times 10^{-1}$
	75				$2.12 \times 10^{-1}$
	105				$2.09 \times 10^{-1}$
	135				$2.08 \times 10^{-1}$
	165				$2.08 \times 10^{-1}$
0.833	15	$4.94 \times 10^{-2}$	$1.94 \times 10^{-1}$	$2.05 \times 10^{-1}$	$2.03 \times 10^{-1}$
	45				$2.00 \times 10^{-1}$
	75				$1.94 \times 10^{-1}$
	105				$1.88 \times 10^{-1}$
	135				$1.88 \times 10^{-1}$
	165				$1.88 \times 10^{-1}$
0.722	15	$4.49 \times 10^{-2}$	$1.76 \times 10^{-1}$	$1.83 \times 10^{-1}$	$1.85 \times 10^{-1}$
	45				$1.82 \times 10^{-1}$
	75				$1.75 \times 10^{-1}$
	105				$1.67 \times 10^{-1}$
	135				$1.67 \times 10^{-1}$
	165				$1.67 \times 10^{-1}$
0.611	15	$3.93 \times 10^{-2}$	$1.54 \times 10^{-1}$	$1.60 \times 10^{-1}$	$1.63 \times 10^{-1}$
	45				$1.61 \times 10^{-1}$
	75				$1.54 \times 10^{-1}$
	105				$1.46 \times 10^{-1}$
	135				$1.45 \times 10^{-1}$
	165				$1.44 \times 10^{-1}$
0.5	15	$3.44 \times 10^{-2}$	$1.35 \times 10^{-1}$	$1.35 \times 10^{-1}$	$1.39 \times 10^{-1}$
	45				$1.37 \times 10^{-1}$
	75				$1.31 \times 10^{-1}$
	105				$1.23 \times 10^{-1}$
	135				$1.21 \times 10^{-1}$
	165				$1.21 \times 10^{-1}$
0.389	15	$2.79 \times 10^{-2}$	$1.09 \times 10^{-1}$	$1.09 \times 10^{-1}$	$1.13 \times 10^{-1}$
	45				$1.11 \times 10^{-1}$
	75				$1.06 \times 10^{-1}$
	105				$9.89 \times 10^{-2}$
	135				$9.67 \times 10^{-2}$
	165				$9.65 \times 10^{-2}$
0.278	15	$2.12 \times 10^{-2}$	$8.31 \times 10^{-2}$	$8.06 \times 10^{-2}$	$8.46 \times 10^{-2}$
	45				$8.30 \times 10^{-2}$
	75				$7.95 \times 10^{-2}$
	105				$7.31 \times 10^{-2}$
	135				$7.05 \times 10^{-2}$
	165				$7.04 \times 10^{-2}$
		$1.60 \times 10^{-2}$	$6.27 \times 10^{-2}$		

Table 5 (contd.)

cosθ	φ (deg)	z (cts.min <sup>-1</sup> .W <sup>-1</sup> )	dα/dΩ (neutrons·ster <sup>-1</sup> per source neutron)		
			Measured	Calculated	
				Isotropic Scattering	Anisotropic Water Scattering <sup>a</sup>
0.167	15	1.41 x 10 <sup>-2</sup>	5.53 x 10 <sup>-2</sup>	4.99 x 10 <sup>-2</sup>	5.33 x 10 <sup>-2</sup>
	45	1.25 x 10 <sup>-2</sup>	4.90 x 10 <sup>-2</sup>		5.21 x 10 <sup>-2</sup>
	75				4.98 x 10 <sup>-2</sup>
	105				4.54 x 10 <sup>-2</sup>
	135	9.47 x 10 <sup>-3</sup>	3.71 x 10 <sup>-2</sup>		4.32 x 10 <sup>-2</sup>
	165				4.31 x 10 <sup>-2</sup>
0.056	15	4.34 x 10 <sup>-3</sup>	1.70 x 10 <sup>-2</sup>	1.66 x 10 <sup>-2</sup>	1.86 x 10 <sup>-2</sup>
	45	4.44 x 10 <sup>-3</sup>	1.74 x 10 <sup>-2</sup>		1.80 x 10 <sup>-2</sup>
	75				1.72 x 10 <sup>-2</sup>
	105				1.55 x 10 <sup>-2</sup>
	135	2.73 x 10 <sup>-3</sup>	1.07 x 10 <sup>-2</sup>		1.45 x 10 <sup>-2</sup>
	165				1.46 x 10 <sup>-2</sup>

a. Average of two runs.

Table 6. Comparison of Calculated Values of  $d\alpha/d\Omega$  with Experiment for  $\theta_0 = 75$  deg

$ \cos\theta $	$\phi$ (deg)	(cts.min <sup>-1</sup> .W <sup>-1</sup> )	$d\alpha/d\Omega$ (neutrons.ster <sup>-1</sup> per source neutron)		
			Measured	Calculated	
				Isotropic Scattering	Anisotropic Water Scattering
0.944	15	$5.61 \times 10^{-2}$	$2.20 \times 10^{-1}$	$2.13 \times 10^{-1}$	$2.16 \times 10^{-1}$
	45				$2.14 \times 10^{-1}$
	75				$2.09 \times 10^{-1}$
	105				$2.04 \times 10^{-1}$
	135				$1.99 \times 10^{-1}$
0.833	15	$5.48 \times 10^{-2}$	$2.15 \times 10^{-1}$	$1.96 \times 10^{-1}$	$1.98 \times 10^{-1}$
	45				$2.04 \times 10^{-1}$
	75				$2.02 \times 10^{-1}$
	105				$1.95 \times 10^{-1}$
	135				$1.86 \times 10^{-1}$
0.722	15	$4.91 \times 10^{-2}$	$1.92 \times 10^{-1}$	$1.79 \times 10^{-1}$	$1.82 \times 10^{-1}$
	45				$1.89 \times 10^{-1}$
	75				$1.86 \times 10^{-1}$
	105				$1.79 \times 10^{-1}$
	135				$1.69 \times 10^{-1}$
0.611	15	$4.41 \times 10^{-2}$	$1.73 \times 10^{-1}$	$1.59 \times 10^{-1}$	$1.64 \times 10^{-1}$
	45				$1.64 \times 10^{-1}$
	75				$1.61 \times 10^{-1}$
	105				$1.50 \times 10^{-1}$
	135				$1.46 \times 10^{-1}$
0.5	15	$3.91 \times 10^{-2}$	$1.53 \times 10^{-1}$	$1.39 \times 10^{-1}$	$1.45 \times 10^{-1}$
	45				$1.48 \times 10^{-1}$
	75				$1.42 \times 10^{-1}$
	105				$1.30 \times 10^{-1}$
	135				$1.26 \times 10^{-1}$
0.389	15	$3.34 \times 10^{-2}$	$1.31 \times 10^{-1}$	$1.16 \times 10^{-1}$	$1.25 \times 10^{-1}$
	45				$1.28 \times 10^{-1}$
	75				$1.25 \times 10^{-1}$
	105				$1.19 \times 10^{-1}$
	135				$1.08 \times 10^{-1}$
0.278	15	$2.73 \times 10^{-2}$	$1.07 \times 10^{-1}$	$8.99 \times 10^{-2}$	$1.04 \times 10^{-1}$
	45				$1.04 \times 10^{-1}$
	75				$9.83 \times 10^{-2}$
	105				$9.30 \times 10^{-2}$
	135				$8.36 \times 10^{-2}$
	165				$7.95 \times 10^{-2}$
	165				$7.92 \times 10^{-2}$

Table 6 (contd.)

cosθ	φ (deg)	z (cts.min <sup>-1</sup> .W <sup>-1</sup> )	dα/dΩ (neutrons·ster <sup>-1</sup> per source neutron)		
			Measured	Calculated	
				Isotropic Scattering	Anisotropic Water Scattering
0.167	15	1.86 x 10 <sup>-2</sup>	7.29 x 10 <sup>-2</sup>	6.02 x 10 <sup>-2</sup>	7.43 x 10 <sup>-2</sup>
	45	1.79 x 10 <sup>-2</sup>	7.02 x 10 <sup>-2</sup>		6.62 x 10 <sup>-2</sup>
	75	1.61 x 10 <sup>-2</sup>	6.31 x 10 <sup>-2</sup>		6.22 x 10 <sup>-2</sup>
	105	1.39 x 10 <sup>-2</sup>	5.45 x 10 <sup>-2</sup>		5.53 x 10 <sup>-2</sup>
	135	1.34 x 10 <sup>-2</sup>	5.25 x 10 <sup>-2</sup>		5.18 x 10 <sup>-2</sup>
	165				
0.056	15	7.22 x 10 <sup>-3</sup>	2.83 x 10 <sup>-2</sup>	2.34 x 10 <sup>-2</sup>	2.99 x 10 <sup>-2</sup>
	45	6.80 x 10 <sup>-3</sup>	2.67 x 10 <sup>-2</sup>		2.51 x 10 <sup>-2</sup>
	75	5.75 x 10 <sup>-3</sup>	2.25 x 10 <sup>-2</sup>		2.35 x 10 <sup>-2</sup>
	105	5.48 x 10 <sup>-3</sup>	2.15 x 10 <sup>-2</sup>		2.05 x 10 <sup>-2</sup>
	135	4.52 x 10 <sup>-3</sup>	1.77 x 10 <sup>-2</sup>		1.88 x 10 <sup>-2</sup>
	165				

measurements of Greenspan and Baksys yields results that agree with the measurements surprisingly well. The latter calculations produce a root mean square deviation of 5.1% from the 72 measured angular albedos.

Table 7 presents values of the differential angular albedos for  $\theta_0 \approx 90$  deg calculated by Monte Carlo. No measurements were made to corroborate these values, but the degree of agreement obtained at other incident angles would indicate a high degree of accuracy in these values.

As far as subcadmium neutron reflection is concerned, the single-velocity treatment thus seems to be quite adequate for concrete. The capture gamma-ray dose albedo, on the other hand, is undoubtedly much more sensitive to the one-velocity approximation. If one is content with estimates of the subcadmium differential angular albedos for reinforced concrete to within  $\pm 40\%$  over the entire incident and backscattering hemisphere, the theory of Chandrasekhar<sup>2</sup> is adequate; the simple expressions of Wells<sup>7</sup> are somewhat less accurate over the complete range of  $\theta_0$ ,  $\theta$ , and  $\phi$ , and fail completely in the vicinity of grazing incidence.

#### IV. SIMPLE ALBEDO EXPRESSIONS

The following four simple expressions are offered as improvements on existing expressions for the differential angular and total albedos from concrete for subcadmium neutrons and capture gamma-ray doses. In all four expressions  $\mu$  and  $\mu_0$  are the polar angle cosines, with respect to an inwardly drawn slab normal, of the reflected and incident beams, respectively, and  $\phi$  is the conventional azimuth depicted in Fig. 1.

---

7. M. B. Wells, Reflection of Thermal Neutrons and Neutron-Capture Gamma Rays from Concrete, RRA-M44, Radiation Research Associates (1964).

Table 7. Calculated Values of  $d\alpha/d\Omega$  for  $\theta_0 \approx 90$  deg

cos $\theta$	$\phi$ (deg)	$d\alpha/d\Omega$ (neutrons $\cdot$ ster $^{-1}$ per source neutron)	
		Isotropic Scattering <sup>a</sup>	Anisotropic Water Scattering
0.944	15	$1.82 \times 10^{-1}$	$1.90 \times 10^{-1}$
	45		$1.88 \times 10^{-1}$
	75		$1.84 \times 10^{-1}$
	105		$1.76 \times 10^{-1}$
	135		$1.70 \times 10^{-1}$
	165		$1.66 \times 10^{-1}$
0.833	15	$1.73 \times 10^{-1}$	$1.86 \times 10^{-1}$
	45		$1.83 \times 10^{-1}$
	75		$1.77 \times 10^{-1}$
	105		$1.65 \times 10^{-1}$
	135		$1.54 \times 10^{-1}$
	165		$1.50 \times 10^{-1}$
0.722	15	$1.63 \times 10^{-1}$	$1.80 \times 10^{-1}$
	45		$1.76 \times 10^{-1}$
	75		$1.68 \times 10^{-1}$
	105		$1.54 \times 10^{-1}$
	135		$1.41 \times 10^{-1}$
	165		$1.40 \times 10^{-1}$
0.611	15	$1.53 \times 10^{-1}$	$1.72 \times 10^{-1}$
	45		$1.67 \times 10^{-1}$
	75		$1.59 \times 10^{-1}$
	105		$1.43 \times 10^{-1}$
	135		$1.30 \times 10^{-1}$
	165		$1.30 \times 10^{-1}$
0.5	15	$1.42 \times 10^{-1}$	$1.71 \times 10^{-1}$
	45		$1.58 \times 10^{-1}$
	75		$1.48 \times 10^{-1}$
	105		$1.31 \times 10^{-1}$
	135		$1.20 \times 10^{-1}$
	165		$1.19 \times 10^{-1}$
0.389	15	$1.31 \times 10^{-1}$	$1.72 \times 10^{-1}$
	45		$1.48 \times 10^{-1}$
	75		$1.37 \times 10^{-1}$
	105		$1.19 \times 10^{-1}$
	135		$1.08 \times 10^{-1}$
	165		$1.08 \times 10^{-1}$
0.278	15	$1.19 \times 10^{-1}$	$1.68 \times 10^{-1}$
	45		$1.36 \times 10^{-1}$
	75		$1.25 \times 10^{-1}$
	105		$1.07 \times 10^{-1}$
	135		$9.60 \times 10^{-2}$
	165		$9.59 \times 10^{-2}$

Table 7 (contd.)

cosθ	φ (deg)	dα/dΩ (neutrons.ster <sup>-1</sup> per source neutron)	
		Isotropic Scattering	Anisotropic Water Scattering
0.167	15	1.05 x 10 <sup>-1</sup>	1.60 x 10 <sup>-1</sup>
	45		1.23 x 10 <sup>-1</sup>
	75		1.12 x 10 <sup>-1</sup>
	105		9.27 x 10 <sup>-2</sup>
	135		8.25 x 10 <sup>-2</sup>
	165		8.24 x 10 <sup>-2</sup>
0.056	15	8.97 x 10 <sup>-2</sup>	1.46 x 10 <sup>-1</sup>
	45		1.07 x 10 <sup>-1</sup>
	75		9.59 x 10 <sup>-2</sup>
	105		7.69 x 10 <sup>-2</sup>
	135		6.69 x 10 <sup>-2</sup>
	165		6.69 x 10 <sup>-2</sup>

For thermal-neutron current albedo:

$$\frac{d\alpha}{d\Omega} = \frac{0.0875|\mu|}{|\mu| + \mu_0} (1 + 1.28|\mu|)(1 + 1.62\mu_0 - 0.42\mu_0^2) \times$$

$$\times [1 + (1 - \mu_0)(1 - |\mu|)(-0.10 + 0.43 \cos\phi + 0.20 \cos^2\phi)] \quad , \quad (1)$$

$$\alpha = 0.86 - 0.19\mu_0 \quad . \quad (2)$$

For capture gamma-ray current dose rate albedo:

$$\frac{dD_\gamma}{d\Omega} = \mu^{2/3}(1.01 + 1.67\mu_0 - 0.56\mu_0^2) \times 10^{-7}$$

$$\text{rads/hr/steradian/incident thermal neutron/sec} \quad , \quad (3)$$

$$D_\gamma = 3.77 \times 10^{-7} (1.01 + 1.67\mu_0 - 0.56\mu_0^2)$$

$$\text{rads/hr/incident thermal neutron/sec} \quad . \quad (4)$$

For the subcadmium neutrons, the differential expression agrees with experiment and calculations to within +10% everywhere, and the total albedo agrees to within +2% of the calculated values at 0, 45, 60, 75, and 90 deg. No experimental verification yet exists for the calculations on which the expressions for the gamma-ray dose rate albedos are based. Somewhat similar expressions have been obtained by Wells.<sup>7</sup> For this concrete composition, accuracies of +15% are attached to the capture gamma-ray dose rate curve fits of the Monte Carlo data.

APPENDIX

Tables A1-A5 reproduce the capture data obtained in the Monte Carlo calculations when the presence of the iron reinforcing was considered. Each table contains the capture distributions within a concrete slab 17 mfp thick ( $z_{\max} \simeq 9$  in.) for each of the two assumed scattering laws. The data were obtained for 2,000 histories and each history was allowed a maximum of 200 scatterings. The residual weights of neutrons scattered more than 200 times contributed only  $\sim 1\%$  to the total capture and were ignored in the tables below.

Table A1. Calculated Capture Distribution for  $\theta_0 = 0$  deg

Neutrons Absorbed per mfp per Source Neutron		
$\Delta z$ (mfp)	Anisotropic Water Scattering <sup>a</sup>	Isotropic Scattering
0-1.0	$3.69 \times 10^{-2}$	$3.59 \times 10^{-2}$
1.0-2.0	$3.84 \times 10^{-2}$	$3.35 \times 10^{-2}$
2.0-2.4	$3.37 \times 10^{-2}$	$2.96 \times 10^{-2}$
2.4-3.0 <sup>b</sup>	$5.38 \times 10^{-2}$	$4.67 \times 10^{-2}$
3.0-4.0 <sup>b</sup>	$4.61 \times 10^{-2}$	$4.11 \times 10^{-2}$
4.0-4.3 <sup>b</sup>	$4.10 \times 10^{-2}$	$3.59 \times 10^{-2}$
4.3-5.0	$2.04 \times 10^{-2}$	$1.99 \times 10^{-2}$
5.0-6.0	$1.70 \times 10^{-2}$	$1.64 \times 10^{-2}$
6.0-7.0	$1.41 \times 10^{-2}$	$1.50 \times 10^{-2}$
7.0-8.0	$1.24 \times 10^{-2}$	$1.28 \times 10^{-2}$
8.0-9.0	$9.94 \times 10^{-3}$	$1.00 \times 10^{-2}$
9.0-10.0	$8.20 \times 10^{-3}$	$7.72 \times 10^{-3}$
10.0-11.0	$6.50 \times 10^{-3}$	$6.20 \times 10^{-3}$
11.0-12.0	$5.61 \times 10^{-3}$	$4.83 \times 10^{-3}$
12.0-13.0	$4.50 \times 10^{-3}$	$3.78 \times 10^{-3}$
13.0-14.0 <sup>b</sup>	$5.53 \times 10^{-3}$	$4.65 \times 10^{-3}$
14.0-14.8 <sup>b</sup>	$4.22 \times 10^{-3}$	$3.86 \times 10^{-3}$
14.8-15.0	$1.78 \times 10^{-3}$	$1.88 \times 10^{-3}$
15.0-16.0	$1.56 \times 10^{-3}$	$1.25 \times 10^{-3}$
16.0-17.0	$7.42 \times 10^{-4}$	$7.01 \times 10^{-4}$

a. Average of two runs.

b. Iron reinforced regions.

Table A2. Calculated Capture Distribution for  $\theta_0 = 45$  deg

Neutrons Absorbed per mfp per Source Neutron		
$\Delta z$ (mfp)	Anisotropic Water Scattering	Isotropic Scattering
0-1.0	$4.03 \times 10^{-2}$	$3.94 \times 10^{-2}$
1.0-2.0	$3.33 \times 10^{-2}$	$3.08 \times 10^{-2}$
2.0-2.4	$2.77 \times 10^{-2}$	$2.75 \times 10^{-2}$
2.4-3.0 <sup>a</sup>	$4.53 \times 10^{-2}$	$4.20 \times 10^{-2}$
3.0-4.0 <sup>a</sup>	$3.95 \times 10^{-2}$	$3.59 \times 10^{-2}$
4.0-4.3 <sup>a</sup>	$3.30 \times 10^{-2}$	$2.96 \times 10^{-2}$
4.3-5.0	$1.73 \times 10^{-2}$	$1.60 \times 10^{-2}$
5.0-6.0	$1.38 \times 10^{-2}$	$1.41 \times 10^{-2}$
6.0-7.0	$1.12 \times 10^{-2}$	$1.12 \times 10^{-2}$
7.0-8.0	$9.78 \times 10^{-3}$	$8.59 \times 10^{-3}$
8.0-9.0	$7.28 \times 10^{-3}$	$6.59 \times 10^{-3}$
9.0-10.0	$6.58 \times 10^{-3}$	$5.53 \times 10^{-3}$
10.0-11.0	$5.86 \times 10^{-3}$	$4.40 \times 10^{-3}$
11.0-12.0	$4.44 \times 10^{-3}$	$3.59 \times 10^{-3}$
12.0-13.0	$3.72 \times 10^{-3}$	$2.81 \times 10^{-3}$
13.0-14.0 <sup>a</sup>	$4.05 \times 10^{-3}$	$3.26 \times 10^{-3}$
14.0-14.8 <sup>a</sup>	$2.85 \times 10^{-3}$	$2.30 \times 10^{-3}$
14.8-15.0	$1.41 \times 10^{-3}$	$1.12 \times 10^{-3}$
15.0-16.0	$1.01 \times 10^{-3}$	$9.63 \times 10^{-4}$
16.0-17.0	$6.89 \times 10^{-4}$	$4.62 \times 10^{-4}$

a. Iron reinforced regions.

Table A3. Calculated Capture Distribution for  $\theta_0 = 60$  deg

Neutrons Absorbed per mfp per Source Neutron		
$\Delta z$ (mfp)	Anisotropic Water Scattering <sup>a</sup>	Isotropic Scattering
0-1.0	$4.07 \times 10^{-2}$	$4.24 \times 10^{-2}$
1.0-2.0	$2.93 \times 10^{-2}$	$2.98 \times 10^{-2}$
2.0-2.4	$2.30 \times 10^{-2}$	$2.27 \times 10^{-2}$
2.4-3.0 <sup>b</sup>	$3.64 \times 10^{-2}$	$3.35 \times 10^{-2}$
3.0-4.0 <sup>b</sup>	$2.97 \times 10^{-2}$	$2.84 \times 10^{-2}$
4.0-4.3 <sup>b</sup>	$2.62 \times 10^{-2}$	$2.46 \times 10^{-2}$
4.3-5.0	$1.36 \times 10^{-2}$	$1.29 \times 10^{-2}$
5.0-6.0	$1.16 \times 10^{-2}$	$1.13 \times 10^{-2}$
6.0-7.0	$9.33 \times 10^{-3}$	$9.19 \times 10^{-3}$
7.0-8.0	$7.96 \times 10^{-3}$	$7.40 \times 10^{-3}$
8.0-9.0	$6.56 \times 10^{-3}$	$6.18 \times 10^{-3}$
9.0-10.0	$5.48 \times 10^{-3}$	$4.61 \times 10^{-3}$
10.0-11.0	$4.42 \times 10^{-3}$	$4.12 \times 10^{-3}$
11.0-12.0	$3.55 \times 10^{-3}$	$3.29 \times 10^{-3}$
12.0-13.0	$3.05 \times 10^{-3}$	$2.62 \times 10^{-3}$
13.0-14.0 <sup>b</sup>	$3.57 \times 10^{-3}$	$3.42 \times 10^{-3}$
14.0-14.8 <sup>b</sup>	$3.00 \times 10^{-3}$	$2.50 \times 10^{-3}$
14.8-15.0	$1.25 \times 10^{-3}$	$1.19 \times 10^{-3}$
15.0-16.0	$1.09 \times 10^{-3}$	$1.11 \times 10^{-3}$
16.0-17.0	$5.46 \times 10^{-4}$	$5.95 \times 10^{-4}$

a. Average of two runs.

b. Iron reinforced regions.

Table A4. Calculated Capture Distributions for  $\theta_0 = 75$  deg

$\Delta z$ (mfp)	Neutrons Absorbed per mfp per Source Neutron	
	Anisotropic Water Scattering	Isotropic Scattering
0-1.0	$4.01 \times 10^{-2}$	$4.05 \times 10^{-2}$
1.0-2.0	$2.18 \times 10^{-2}$	$2.25 \times 10^{-2}$
2.0-2.4	$1.89 \times 10^{-2}$	$1.75 \times 10^{-2}$
2.4-3.0 <sup>a</sup>	$3.13 \times 10^{-2}$	$2.77 \times 10^{-2}$
3.0-4.0 <sup>a</sup>	$2.47 \times 10^{-2}$	$2.09 \times 10^{-2}$
4.0-4.3 <sup>a</sup>	$2.13 \times 10^{-2}$	$1.90 \times 10^{-2}$
4.3-5.0	$1.18 \times 10^{-2}$	$1.00 \times 10^{-2}$
5.0-6.0	$9.97 \times 10^{-3}$	$8.78 \times 10^{-3}$
6.0-7.0	$8.01 \times 10^{-3}$	$7.02 \times 10^{-3}$
7.0-8.0	$6.89 \times 10^{-3}$	$6.14 \times 10^{-3}$
8.0-9.0	$5.69 \times 10^{-3}$	$5.25 \times 10^{-3}$
9.0-10.0	$4.83 \times 10^{-3}$	$4.03 \times 10^{-3}$
10.0-11.0	$3.81 \times 10^{-3}$	$3.13 \times 10^{-3}$
11.0-12.0	$3.15 \times 10^{-3}$	$2.30 \times 10^{-3}$
12.0-13.0	$2.48 \times 10^{-3}$	$1.78 \times 10^{-3}$
13.0-14.0 <sup>a</sup>	$2.98 \times 10^{-3}$	$2.55 \times 10^{-3}$
14.0-14.8 <sup>a</sup>	$2.21 \times 10^{-3}$	$1.70 \times 10^{-3}$
14.8-15.0	$1.12 \times 10^{-3}$	$7.88 \times 10^{-4}$
15.0-16.0	$6.70 \times 10^{-4}$	$7.19 \times 10^{-4}$
16.0-17.0	$4.53 \times 10^{-4}$	$3.69 \times 10^{-4}$

a. Iron reinforced regions.

Table A5. Calculated Capture Distributions for  $\theta_0 = 90$  deg

Neutrons Absorbed per mfp per Source Neutron		
$\Delta z$ (mfp)	Anisotropic Water Scattering	Isotropic Scattering
0-1.0	$3.08 \times 10^{-2}$	$3.15 \times 10^{-2}$
1.0-2.0	$1.37 \times 10^{-2}$	$1.34 \times 10^{-2}$
2.0-2.4	$1.19 \times 10^{-2}$	$1.14 \times 10^{-2}$
2.4-3.0 <sup>a</sup>	$1.82 \times 10^{-2}$	$1.80 \times 10^{-2}$
3.0-4.0 <sup>a</sup>	$1.66 \times 10^{-2}$	$1.55 \times 10^{-2}$
4.0-4.3 <sup>a</sup>	$1.48 \times 10^{-2}$	$1.25 \times 10^{-2}$
4.3-5.0	$7.47 \times 10^{-3}$	$6.17 \times 10^{-3}$
5.0-6.0	$6.12 \times 10^{-3}$	$5.57 \times 10^{-3}$
6.0-7.0	$4.72 \times 10^{-3}$	$4.48 \times 10^{-3}$
7.0-8.0	$3.65 \times 10^{-3}$	$3.88 \times 10^{-3}$
8.0-9.0	$3.14 \times 10^{-3}$	$3.05 \times 10^{-3}$
9.0-10.0	$2.42 \times 10^{-3}$	$2.73 \times 10^{-3}$
10.0-11.0	$2.26 \times 10^{-3}$	$2.23 \times 10^{-3}$
11.0-12.0	$1.63 \times 10^{-3}$	$1.64 \times 10^{-3}$
12.0-13.0	$1.34 \times 10^{-3}$	$1.55 \times 10^{-3}$
13.0-14.0 <sup>a</sup>	$1.54 \times 10^{-3}$	$1.94 \times 10^{-3}$
14.0-14.8 <sup>a</sup>	$1.39 \times 10^{-3}$	$1.12 \times 10^{-3}$
14.8-15.0	$4.82 \times 10^{-4}$	$6.65 \times 10^{-4}$
15.0-16.0	$5.65 \times 10^{-4}$	$5.57 \times 10^{-4}$
16.0-17.0	$3.10 \times 10^{-4}$	$3.65 \times 10^{-4}$

a. Iron reinforced regions.

ORNL-4090  
UC-80 - Reactor Technology

## INTERNAL DISTRIBUTION

- |                                      |                                 |
|--------------------------------------|---------------------------------|
| 1. Biology Library                   | 155-159. R. E. Maerker          |
| 2-4. Central Research Library        | 160. H. G. MacPherson           |
| 5-6. ORNL - Y-12 Technical Library   | 161. F. C. Maienschein          |
| Document Reference Section           | 162-166. F. J. Muckenthaler     |
| 7-146. Laboratory Records Department | 167. R. W. Peelle               |
| 147. Laboratory Records, ORNL R.C.   | 168. A. M. Perry                |
| 148. L. S. Abbott                    | 169. M. J. Skinner              |
| 149. J. A. Auxier                    | 170. E. Straker                 |
| 150. C. E. Bettis                    | 171. D. K. Trubey               |
| 151. V. R. Cain                      | 172. A. M. Weinberg             |
| 152. C. E. Clifford                  | 173. G. Dessauer (consultant)   |
| 153. L. B. Holland                   | 174. B. C. Diven (consultant)   |
| 154. W. H. Jordan                    | 175. M. H. Kalos (consultant)   |
| 155. C. E. Larson                    | 176. L. V. Spencer (consultant) |

## EXTERNAL DISTRIBUTION

177. J. A. Swartout, Union Carbide Corporation, New York, N.Y.  
178. P. B. Hemmig, Division of Reactor Development and Technology,  
U.S. Atomic Energy Commission, Washington, D.C.  
179. I. F. Zartman, Division of Reactor Development and Technology,  
U.S. Atomic Energy Commission, Washington, D.C.  
180. Herbert Goldstein, Columbia University, Mudd Building, New York, N.Y.  
181. Research and Development Division, AEC, ORO  
182-459. Given distribution as shown in TID-4500 under Reactor Technology  
category (25 copies - CFSTI)